Photovoltaic Sub-module Integrated Converter Analysis

by

Sourav Sen

A Thesis Presented in Partial Fulfillment
of the Requirements for the Degree
Master of Science

Approved June 2012 by the
Graduate Supervisory Committee:

Raja Ayyanar, Chair
Sayfe Kiaei
Bertan Bakkaloglu

ARIZONA STATE UNIVERSITY

August 2012

ABSTRACT

With the rapid expansion of the photovoltaic industry over the last decade, there has been a huge demand in the PV installations in the residential sector. This thesis focuses on the analysis and implementation of a dc-dc boost converter at photovoltaic sub-module level. The thesis also analyses the various topologies like switched capacitors and extended duty ratio which can be practically implemented in the photovoltaic panels. The results obtained in this work have concentrated on the use of novel strategies to substitute the use of central dc-dc converter used in PV module string connection. The implementation of distributed MPPT at the PV sub-module level is also an integral part of this thesis.

Using extensive PLECS simulations, this thesis came to the conclusion that with the design of a proper compensation at the dc interconnection of a series or parallel PV Module Integrated Converter string, the central dc-dc converter can be substituted. The dc-ac interconnection voltage remains regulated at all irradiance level even without a dc-dc central converter at the string end. The foundation work for the hardware implementation has also been carried out. Design of parameters for future hardware implementation has also been presented in detail in this thesis.

ACKNOWLEDGMENTS

First and foremost, I would like to offer my sincere gratitude to my advisor, Dr. Raja Ayyanar, whose guidance and support from the start to the final days of the thesis helped me develop an understanding of the subject. I attribute my Master's degree to his encouragement and effort without which this thesis could not have been completed. One simply could not wish for a more supportive supervisor.

I also want to express my gratitude to Dr. Sayfe Kiaei and Dr. Bertan Bakkaloglu for their time and consideration for being a part of my graduate supervisory committee and guiding me whenever I needed any advice. The financial assistance provided by the ASU Light Works for this thesis must also be greatly acknowledged.

I take this opportunity to thank my parents Mr. Soumitra Sen and Mrs. Japamala Sen who helped me pursue all my goals throughout my career. I would also like to thank my friends who stood by me and encouraged me all the time.

TABLE OF CONTENTS

CHAPTER PAGE

LIST OF FIGURES

FIGURE PAGE

FIGURE PAGE

FIGURE PAGE

FIGURE PAGE

NOMENCLATURE

PV	Photovoltaic
MIC	Module integrated converter
LCOE	Levelized cost of energy
NREL	National renewable energy laboratory
DOE	Department of energy
RPS	Renewable portfolio standards
CSP	Concentrated solar power
MPPT	Maximum power point tracking
AC	Alternating current
DC	Direct current
RMS	Root mean square
MPP	Maximum power point
IC	Incremental conductance
OC	Open circuit
ISC	Short circuit current
SC	Switched capacitors
EMI	Electromagnetic interference
BOM	Bill of material

Chapter 1. Introduction to Solar Energy and PV industry

1.1 PV industry present scenario

Coal and natural gas electrical power stations are significant generators of electricity in the United States. Nearly 90% of the installed generation capacity in the United States is composed of dispatchable natural gas, coal, and nuclear power resources. These are the conventional sources of electrical energy which have stayed unparalleled and unrivaled. They are reliable and stable. With the finite resources of coal and natural gas dwindling every day, the authorities have realized that they cannot bank on these two resources only for the generation of electricity. These two resources have also come under heavy criticism for the release of greenhouse gases in the atmosphere which are the by-products of any coal or natural gas power plants. Hence there is immediate need for alternatives which can counter this.

Although the solar power plants have been around for some time now, it still has to win the level of acceptability or attain the level of penetration which the conventional power has. The broad reasons for this are the high level of generation intermittency associated with these renewable energy resources, the high installation cost, and price volatility, especially for the solar power plants. Solar power generators and green utilities are working incessantly on this The main motivation for them is to increase the output yield of solar power plants making them more cost attractive for the customers.

Over the last decade solar manufacturing costs have dropped dramatically and so have the sales prices in United States and other countries. Moreover, the huge impetus in research and development (R&D) by NREL and DOE with market stimulation given by the introduction of renewable portfolio standards (RPS) in many states across the country, solar manufacturers and utilities have become more experienced in installing fully operational solar systems in shortened time and expense [1]. Arizona with a huge potential in solar, has set aside a RPS goal of 15% by 2020. California has a more ambitious target of 33%. The photovoltaic (PV) and the concentrated solar power plant (CSP) market has greatly evolved over the last decade. Federal and state policies in U.S. have helped in driving the PV market considerably. Figure 1.1 shows the annual growth in installed grid-connected PV from 2001 to 2010 in U.S. which includes residential and commercial applications.

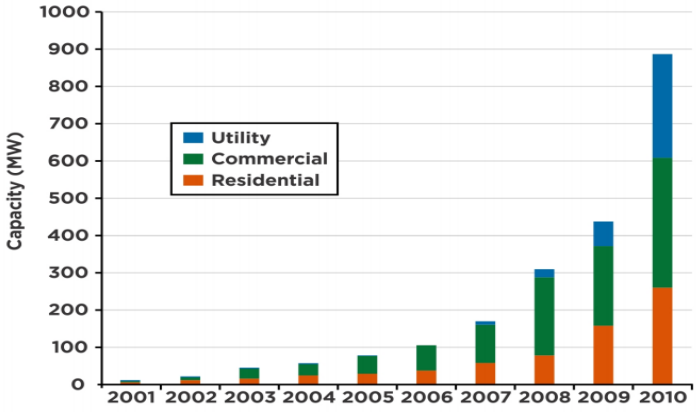

Figure 1.1 U.S.annual installed grid-connected PV capacity by market [1]

1.2 Solar energy resources in the U.S.

Solar power has seen substantial growth in the past decade but still a lot of initiatives need to be taken to keep it an attractive proposition. PV systems in Arizona are currently cost competitive with conventional electrical utilities only in a small scale. A PV system as small as 2 kW can power a small house with low functionality but even after taking the amortization rate, the selling price of PV power stays at 20-25 cents/ kWh as compared to the conventional power currently selling at 10 cents/kWh [2]. Hence more steps needs to be taken to bring about the energy parity.

It has been often stated in many literature that there is abundant solar resource across the United States to exploit. It is about 1000-2500 kWh/m^2/year. The southwestern region of U.S. has the maximum potential. The solar resources throughout the country are more homogeneously laid out compared to other renewable resources. Moreover according to estimates, only 0.6% of the total land is needed in U.S. to power all end-users with PV generated electricity. The pressure on the land utilization is also minimal [1].

With the pressure on land in the U.S. being minimal, a lot of new large scale solar farms are coming up all across the country. Topaz solar farm, a 550 MW centralized PV plant is nearing completion in California with the commissioning date kept as year 2014. In Arizona too, Aqua Caliente, a 290 MW PV plant is coming up around the same time. There are many more PV and CSP plants in the

pipeline over the next 5 years. At the end the system planners will be responsible for the adequate utilization of the huge solar resources and make them operational. According to the SunShot Vision Study undertaken by DOE, the cumulative solar installed capacity by the year 2030 will be 329 GW within the United States. Out of this the total PV contribution in this will be 302 GW. While the Utility PV will be contribute 181 GW in total PV, the rooftop PV, which is expected to grow substantially, will account for 121 GW [1].

1.3 PV market trend

By 2020, residential rooftop PV will have installed system prices of $\$1.50/W_{dc}$ with the commercial rooftop PV at $\$1.25/W_{dc}$. These values are dependent on the analogous decrease in the PV manufacturing technology prices. It is evident in the Figure 1.2 that the electricity generation is evolving towards this trend.

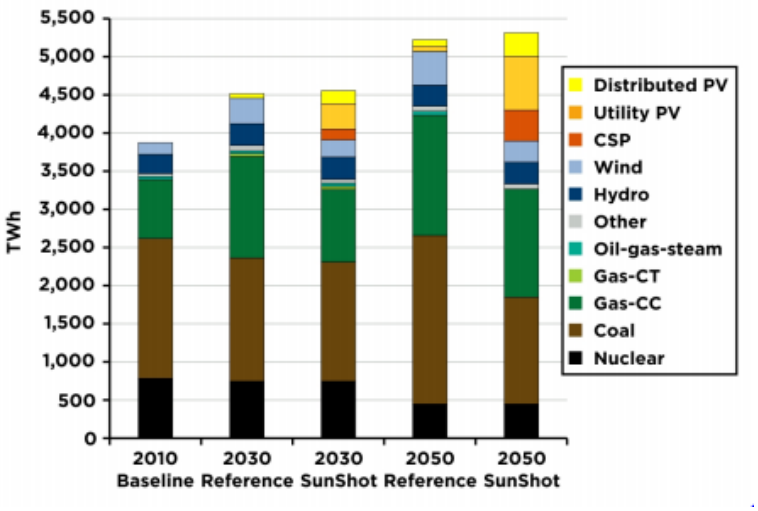

Figure 1.2 Electricity evolution with time [1]

From the figure above, it is obvious that with the increase in the solar electricity generation the cost will go down. But at the same time the price of the PV module manufacturing has to go down. The prices of the photovoltaic module have decreased significantly over the last three decade by almost 20%. At present a typical module price ranges from at around $1.5-$2/W. Figure 1.3 shows this trend to continue in the years to come.

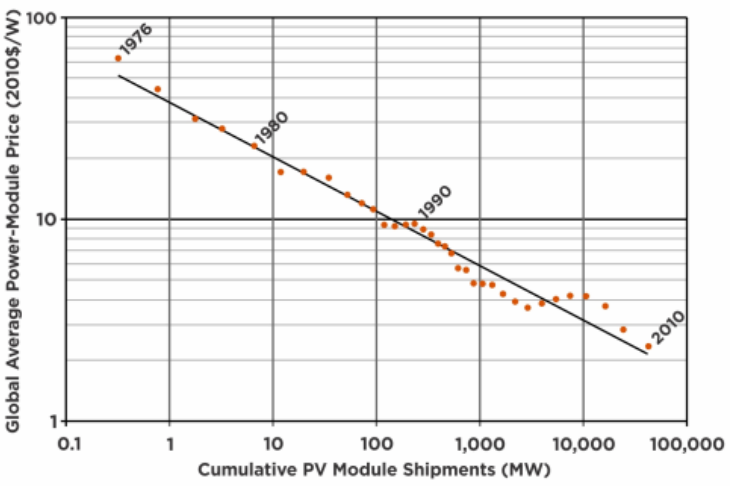

Figure 1.3 Declining factory prices of PV modules [1]

In 2010, the installed price of a commercial PV was around $5/W with the residential system at around 25% more [18]. But with the increase in residential installations and federal incentives these prices are bound are go down over the long run. The levelized cost of energy (LCOE), taking into account the continued incentives is around $0.15-$0.20/kWh for residential systems. To achieve the installed prices for the roof-top PV system as discussed earlier can only be achieved by reducing the installation prices or increasing the system efficiency. This is where power electronics has a crucial role.

While the manufacturing cost of the PV module is decreasing steadily, the PV module efficiencies have been on the rise. The PV cell efficiency has increased consistently over the years. Most of the PV module technologies have shown improvement over the years. Thin film technology especially the cadmium telluride PV cells have improved this outlook. Figure 1.4 shows the various prospects.

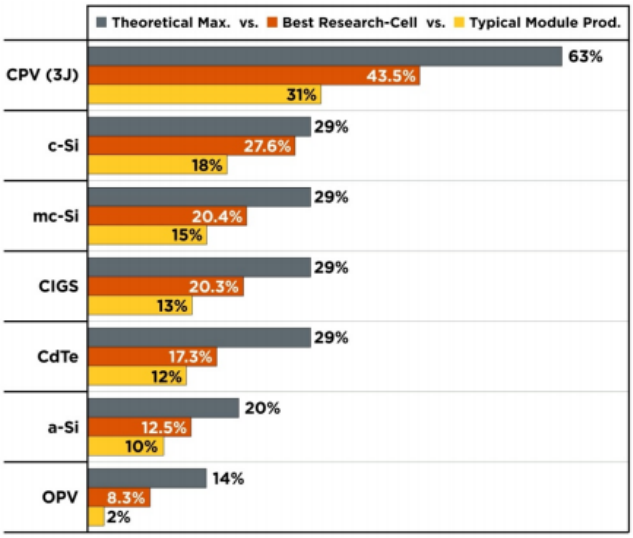

Figure 1.4 Production, laboratory and theoretical PV module efficiencies [1]

While research continues in this field, the other area which is important for the reduction in the cost of the PV energy is the power electronics cost. Inverters, converting dc power produced by the PV modules into AC electricity are priced at around $0.40/W for residential systems. To achieve the installed targets set aside by the DOE SunShot initiative, the inverter price has to come down to $0.12/W level. This can be achieved by addressing the issues of reliability failure during the PV grid integration, developing micro-inverter modules with reduced installation cost, improving MPPT and by advances in dc-dc converter switches using

silicon carbide and gallium nitride. With the implementation of IEEE 1547 standards the grid interconnection of the PV inverters has been regulated. With further modifications and improvement in this guideline, the process of PV installation in the residential sector especially, can be further streamlined.

1.4 PV arrays and inverter

PV arrays

A PV system is no different than any other power generating systems. Instead of the conventional electromechanical systems, there are large arrays of PV module which generate the power in DC power. After the energy conversion and conditioning process, the power generated is converted into ac and fed to the grid or the residential system. The principles of operation and interfacing are well established by electrical codes and standards as mentioned earlier. Figure 1.5 shows the major components of the PV system.

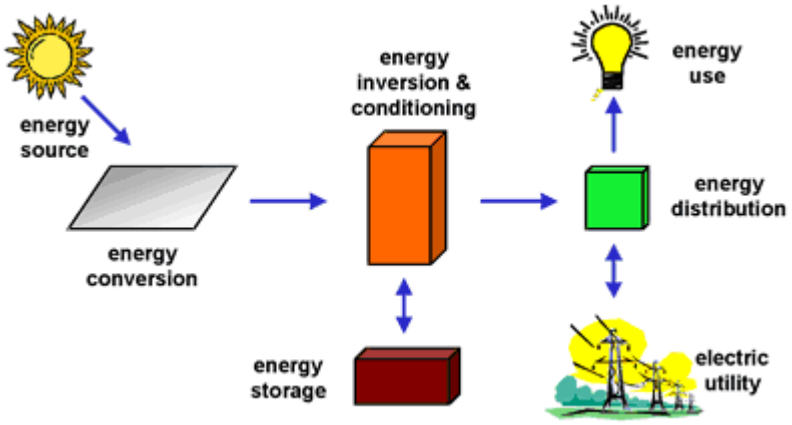

Figure 1.5 Major photovoltaic components [18]

Depending on the functional and operational requirements of the system, the specific components required may include DC-AC power inverter, battery bank, system and battery controller, auxiliary energy sources and sometimes the specified electrical load (appliances). In addition, an assortment of balance of system (BOS) hardware, including wiring, over-current, surge protection and disconnect devices, and other power processing equipment. In this thesis the main concentration will be on the energy conversion and the inversion system.

The energy conversion in the solar panels is done by the converters which are either on the panel or completely centralized. Solar panels used to power homes and businesses are typically made from solar cells combined into modules that hold about 40 cells. A typical home will use about 10 to 20 solar panels to power the home. Many solar panels combined together to create one system is called a solar array. For large electric utility or industrial applications, hundreds of solar arrays are interconnected to form a large utility-scale PV system.

An individual PV cell is usually small, typically producing about 1 or 2 watts of power. To boost the power output of PV cells, they are connected together to form larger units called modules. Modules, in turn, can be connected to form even larger units called arrays, which can be interconnected to produce more power, and so on. In this way, PV systems can be built to meet almost any electric power need, small or large. Figure 1.6 shows the components of a PV array.

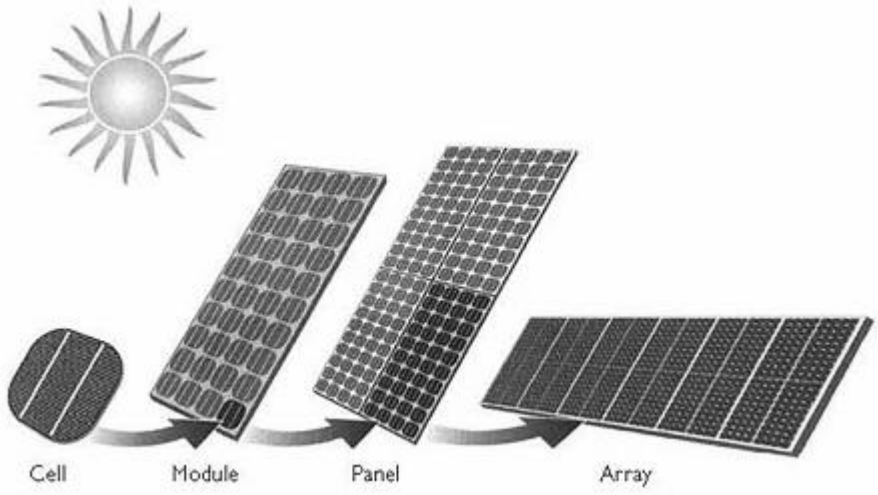

Figure 1.6 Components of PV array [18]

Inverters

The inverter is another crucial component of the PV system. Its main operation includes energy inversion and power conditioning. The inverters work by inverting the dc power generated by the PV modules or arrays into ac. This ac power needs to be integrated to the grid or be used at residential and commercial complexes directly. The two basic types of inverters used for this interconnection are: unipolar inverters and bipolar inverters. The various single-phase inverters used in North America range from 3 kW to 7 kW. With the implementation of IEEE 1547, the PV inverters need to perform more. As solar penetration increases, voltage tolerance or low voltage ride through (LVRT) capability will be required from the PV power plants [1]. Also during high-penetration scenarios, solar plants should also provide reactive support of a character similar to conven-

tional power plants. The PV inverters are expected to provide this solution along with maintaining the power quality.

PV array – inverter configurations

The main focus of the power electronics research is on the PV module and inverter combination. At present, the conventional central inverters for large PV array fields are the most prevalent. In the central inverter architecture, all the PV modules are connected to a central dc-dc converter stage which performs the MPPT and then to an inverter to connect to the utility grid. Although this system seems practical for large scale PV fields, this configuration has its own level of drawbacks. The major problem in this configuration is the loss of energy yield due to the global MPPT tracking failure. Due to partial shading, this configuration has many local MPPs in the system PV plot. The central MPPT at the dc-dc converter fails to recognize the system Global MPP, leading to system energy loss.

With the increase in localization of the inverter from the central array level to the module level, there are many positives. The distribution of the dc-dc converter to string or module level improves the MPPT tracking resulting in improved efficiency and power output yield. With the implementation of distributed MPPT architecture in the string and module inverter level, the partial shading mismatch conditions across the string or modules can be tackled more efficiently. Figure 1.7 shows the various PV modules-inverter configurations which are used at present.

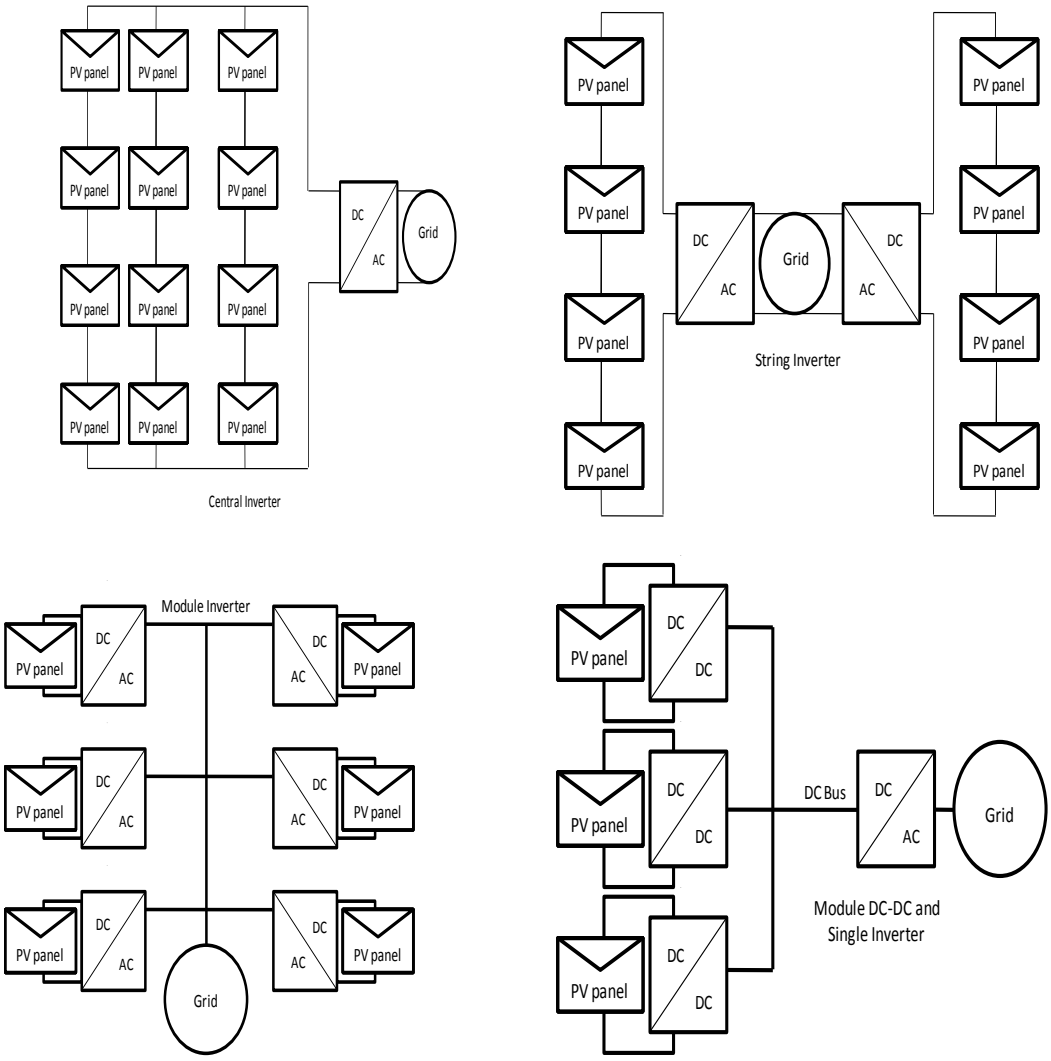

Figure 1.7 Various PV modules-inverter configurations

With improvement in the power electronics, the localization of the dc –dc converter can extend to the individual PV cell level. But this will lead to more complexity and topological constraints. Figure 1.8 shows the dc-dc converter at the PV cellular level.

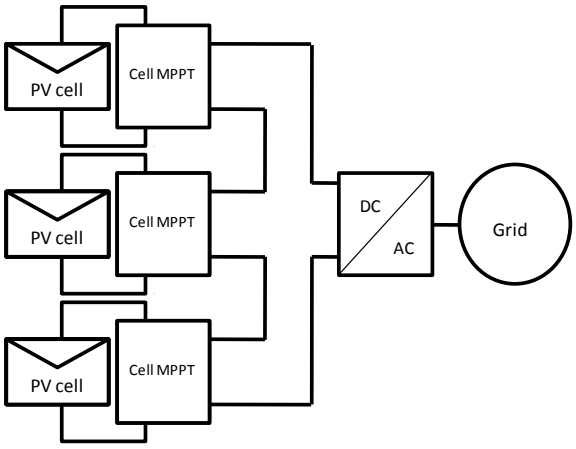

Figure 1.8 PV cell level power electronics implementation

The efficiency of such a system might be best theoretically, with each cell having its individual MPPT to deliver maximum power at any irradiance, but the cost of such an intricate may be prohibitive. This system will gain more acceptability when the performance of such system offsets its cost. If a dc-dc converter for such sub-modular system needs to replace the bypass diode, ideally the cost of that dc-dc converter must be less than that of diode (0.1cent/W) [1]. Moreover, if the dc-dc converters do take up the place of the bypass diodes, they need to be extremely reliable. Any module level inverter solution will render a level of inflexibility to an installer, unlike the central inverter configuration.

1.5 Thesis Objective

The main objective of this thesis is to analyze and experiment with boost dc-dc converter at PV sub-module level. The various novel converter topologies compatible at the sub-module level will also be reviewed. The voltage regulation of the series and parallel connected MICs at the sub-module level operating at different values of irradiance will also be studied. The idea of this study is to verify the adaptability of the MPPT algorithm at the sub-module level and to check whether this system stays regulated and valid even without the addition of any central dc-dc converter at the module string ends.

1.6 Thesis Layout

The chapter 2 in this thesis reviews the PV modeling and characterization discussed in various literatures. It also reviews the incremental conductance MPPT algorithm with focus at the distributed sub-module level implementation. Chapter 3 focuses on module integrated converters and the novel dc-dc converter topologies which can be used at the PV sub-module level. Chapter 4 analyses the implementation of the boost converter at the sub-module level. Using PLECS simulation tool, voltage regulation and the d-MPPT at the sub-module level are thoroughly studied. In the chapter 5, the series and parallel MIC configurations are studied with extensive simulations carried out in PLECS. The foundation of the hardware implementation is laid out in conclusion with focus on the future work.

Chapter 2. PV Modeling and MPPT Algorithm

2.1 PV cell basics

A PV cell, the building blocks of any PV module is a semiconductor device having a p-n junction which works on the principle of converting the light energy from the sun into electrical energy. Figure 2.1 shows the schematic representation of a photovoltaic cell. This is a simplified single-diode model.

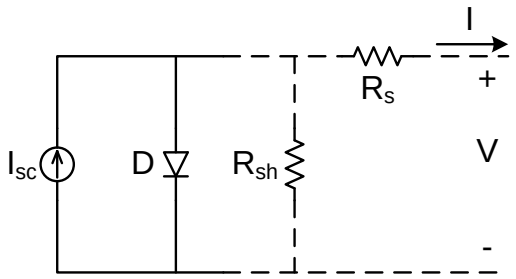

Figure 2.1 Single diode model of a photovoltaic cell.

The PV cell shown in the above figure has a current source which represents the photocurrent generated in it. The diode represents the p-n junction having non-linear impedance. The R_{sh} and R_s are the other parameters of the cell which represent the intrinsic characteristics of the cell. The value of the parallel impedance R_{sh} is typically very high while the value of the series resistance R_s is low. The single-diode model of the PV cell is represented by a mathematic model for the purpose of analysis. The model which represents a PV module is given by:

$$I_{pv} = I_{ph} - I_O\left(e^{\frac{q(V+I_{pv}R_S)}{aKT}} - 1\right) - \left(\frac{V + I_{pv}R_S}{R_{sh}}\right) \quad (2.1)$$

where I_{pv} is the total photovoltaic current generated in the PV module and V denotes the instantaneous PV voltage at the output terminal of the PV module. I_{ph} is the light generated current and I_o is the dark saturation current. I_o is denoted by

$$I_O = \frac{I_{sc}}{\left(e^{\frac{V_{OC}}{V_T}} - 1\right)} \quad (2.2)$$

Here V_T is represented by $V_T = \frac{nN_SKT}{q}$ where N_S stands for the number of cells in the PV module. In the simulations carried out in this research, there are 24 cells in each sub-module. K is the Boltzmann's constant and the q is the charge of an electron (coul). The value of the R_S for each sub-module is obtained by taking the value of R_S of the total PV module and dividing it equally among the sub-modules. The PV sub-module simulation used in PLECS as a part of the project is given by the following Figure 2.2**.**

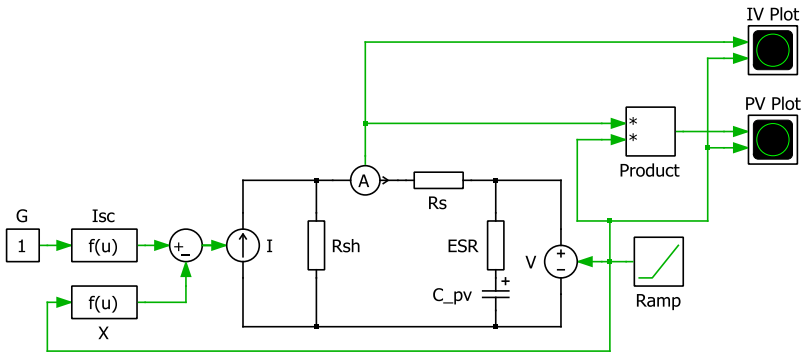

Figure 2.2 PLECS representation of the PV cell

The value of R_S is thus taken as 0.1152 Ω. The value of R_{sh} is typically very high. In the simulation the value is put as100 kΩ. In the Figure 2.2 the function block X is given by $I_O\left(e^{\frac{V}{V_T}}-1\right)$ and the net current source I is defined as $I = GI_{SC} - I_O\left(e^{\frac{V}{V_T}}-1\right)$. This model enables a simpler approach in simulating the PV sub-module model.

The I-V and the P-V characteristics of a PV sub-module represent the change in its characteristics of power output yield and current with respect to the PV sub-module voltage for a given value of irradiance. The I-V and P-V plots for PV sub-module at G=1 and G=0.5 used in the research PLECS model are given in the following Figure 2.3 and Figure 2.4.

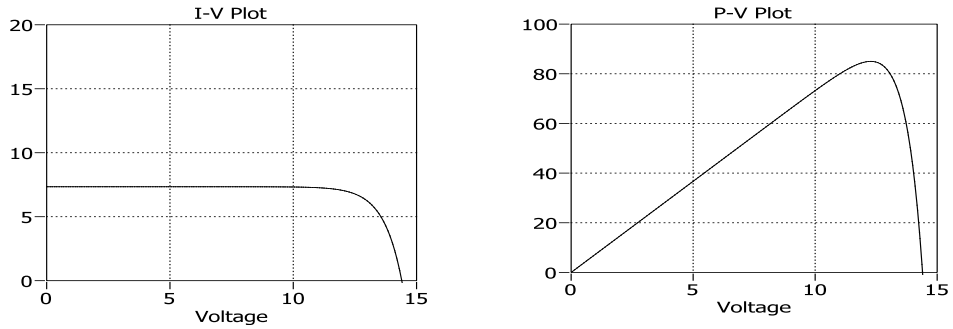

Figure 2.3 (a) I-V plot and (b) P-V plot at irradiance G=100%.

The Y-axis in Figure 2.3(a) is PV sub-module current and in Figure 2.3(b) it stands for PV sub-module output power. The PV sub-module is defined as a group of PV cells connected in series in a PV panel used for integrating the sub-module integrated converter.

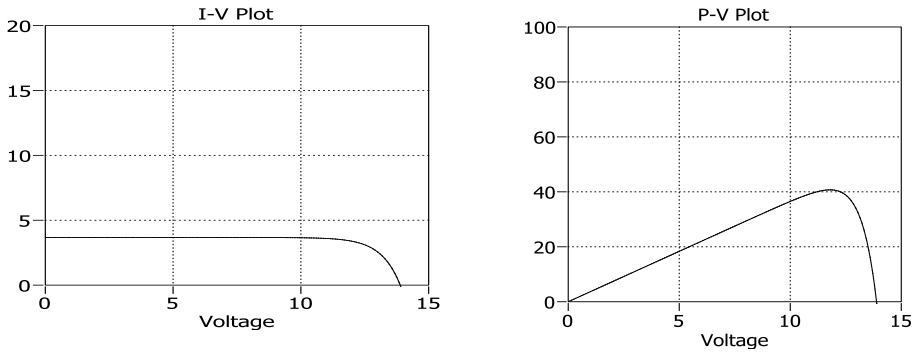

Figure 2.4 (a) I-V plot and (b) P-V plot at irradiance G=50%

2.2 PV sim-electronics model

Figure 2.5 shows the SIM-ELECTRONICS model of a 36 cell PV module. This model helps in understanding the working of the PV cell. In this figure the 36 cell PV module is studied for the impact of the partial shading.

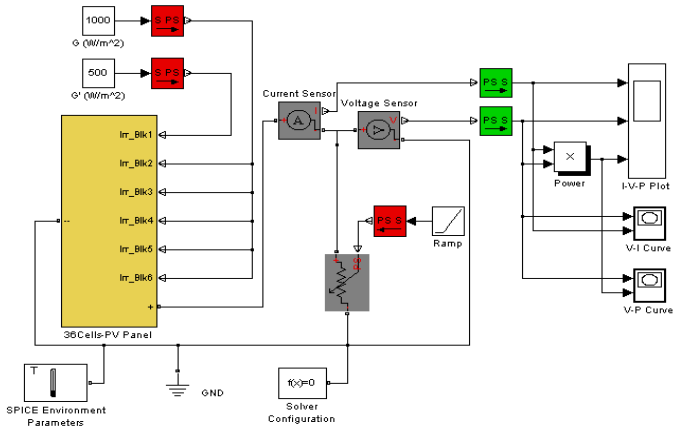

Figure 2.5 PV panel SIM-ELECTRONICS model

Inside the SIM-Electronics model of the 36 PV panel, 6 PV cells are group into one PV sub-module. Each sub-module has an irradiance of G =1000 W/m^2 ex-

cept for one sub-module. The sub-module block is partially shaded with G = 500 W/m^2. Figure 2.6 shows a single PV sub-module and two groups of 18 cell sub-module.

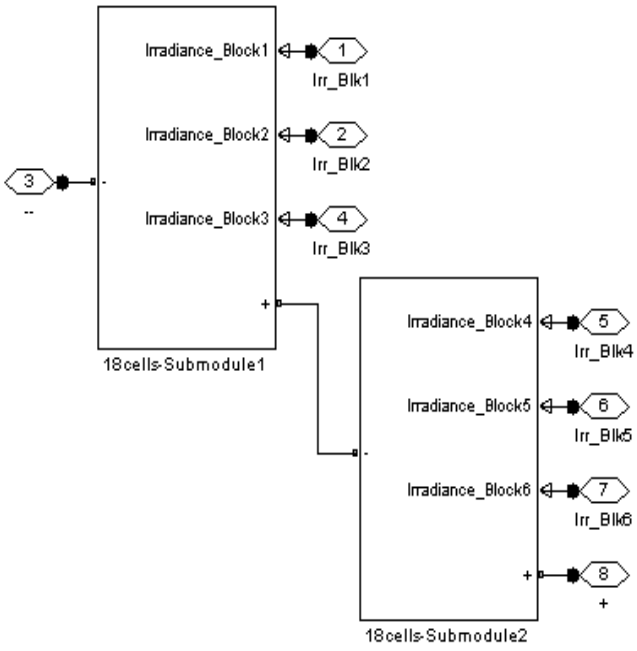

Figure 2.6 (a) 18-cell PV sub-module

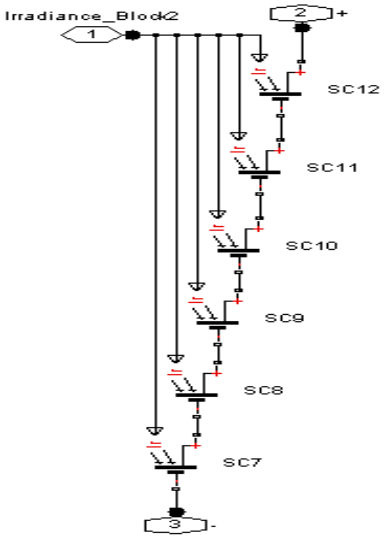

Figure2.6 (b) 6-cells sub-module

The Figure 2.7 shows the P-V and the V-I curve of the PV panel. As mentioned earlier only one sub-module is partially shaded in this model.

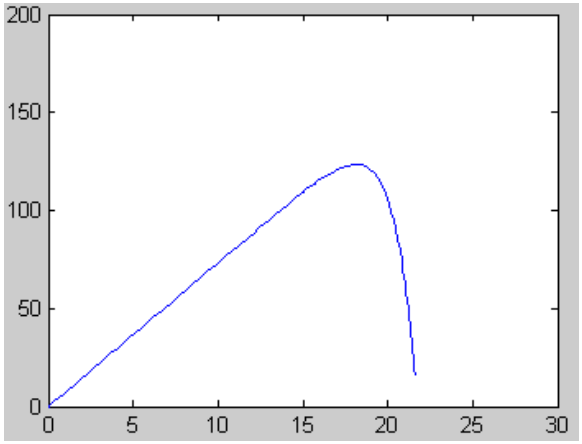

Figure 2.7 (a) P-V plot of entire panel without partial shading. Y-axis represents the net output power and X-axis the panel output voltage.

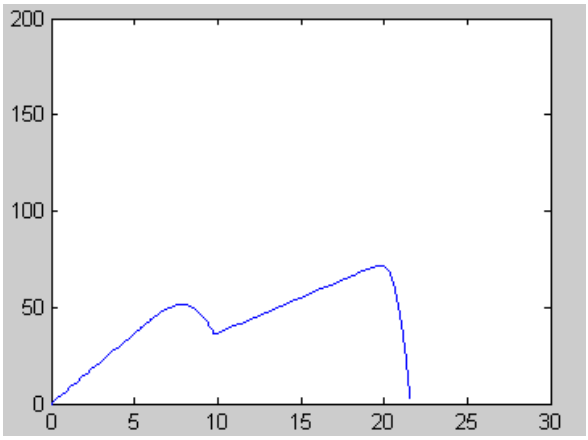

Figure 2.7 (b) P-V plot of the entire panel with partial shading. Y-axis represents the net output power and X-axis the panel output voltage.

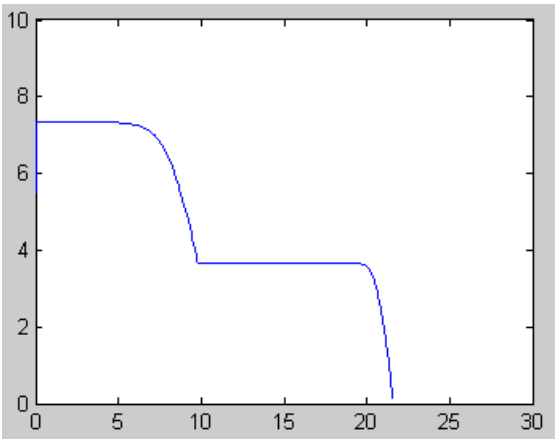

Figure 2.7 (c) I-V plot of the PV panel with partial shading. The X-axis represents the panel output voltage and the Y-axis represents the net panel current.

It is evident from the figures above; that with the absence of sub-module level integrated converter makes the PV panel operates sub-optimally. During unshaded condition, the entire power output of the PV panel is 130 W. When one sub-module is partially shaded with G = 500 W/m^2, the power output of the entire

PV panel drops by almost 50% with two local MPP points. The presence of two local maxima in the P-V plot during the partial shading condition also underlines the importance of the implementation of the module level integrated converter with MPPT control.

2.3 Incremental Conductance Algorithm

The function of the MPPT algorithm is to continuously tune the system so that the converter draws the maximum power from the PV array regardless of weather and load conditions. Since the PV array has non-ideal voltage-current characteristics and the conditions such as irradiance, ambient temperature, and wind that affect the PV output of are unpredictable, a dynamic tracker, rather than a regulator that controls the voltage in a pre-determined way, should be used to ensure the maximum power output. The conventional MPPT algorithms check for $dP/dV = 0$ to reach the maximum power point. The two most frequently used MPPT algorithms are perturb and observe algorithm and the incremental conductance algorithm. The incremental conductance algorithm has been used in this work. It performs better in tracking rapid increase and decrease of irradiance conditions than the perturb and observe algorithm [12].

The incremental conductance algorithm works on the principle of determination of the slope of the PV curve. The maximum power point (MPP) of the curve is reached when the slope of the PV curve is theoretically zero. The operating point moves towards the MPP with the increase in slope and moves away from it

as the slope of the PV curve turns negative. This can be better enumerated by the following [6]

$$\Delta I/\Delta V = I/V \qquad \text{at MPP} \tag{4.1}$$

$$\Delta I/\Delta V = -I/V \quad \text{left of MPP}$$

$$\Delta I/\Delta V = -I/V \quad \text{right of MPP}$$

The important part of the above equations and the flowchart given in Figure 2.8 is the calculation of the instantaneous conductance value (I/V) and the incremental conductance value $\Delta I/\Delta V$. The incremental conductance algorithm calculates the V_{ref} for the PV module voltage V_{pv} in a single iteration and the process continues till the condition for MPP is reached. At the end of a single iteration the value of the V_{ref} is compared with the value of V_{MPP} at the maximum power point. This process continues until the value of the V_{ref} equals V_{MPP}. When V_{ref} equals V_{MPP}, the maximum power yield point from the module is reached and the module operation is maintained at this point. The PV module continues to operate in this point unless there is a sudden change in irradiance, resulting in change in photovoltaic current ΔI. As soon as this change in current is noted, the IC algorithm initiates another sets of iteration until the V_{ref} reaches (increases or decreases) and equals the new V_{MPP} value, in accordance to the new atmospheric conditions. Figure 2.8 shows the incremental conductance algorithm flowchart.

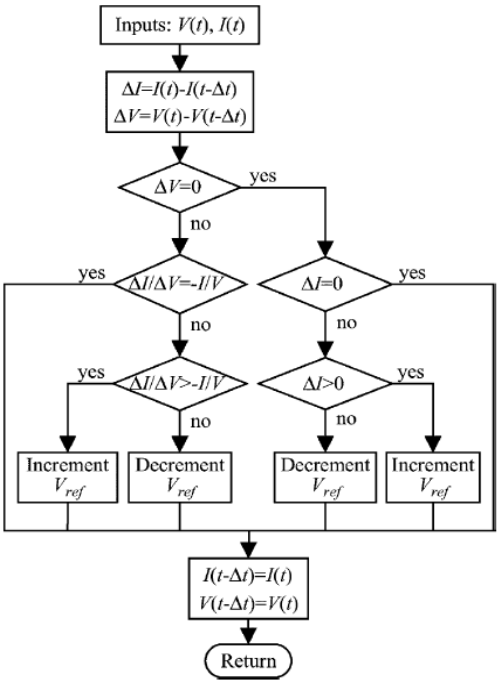

Figure 2.8 Incremental conductance flowchart [5]

With the working of the algorithm explained, this part will concentrate on the optimization steps necessary while deciding the step size of the V_{ref}. The rate at which the V_{ref} tracks the instantaneous V_{MPP} depends on the step size of the increment or decrement. If the step size is increased V_{ref} will track V_{pv} faster but then the stability of the PV system at the MPP will be compromised. So there is a compromise between the dynamics of the algorithm and the stability of the algorithm at MPP [3].

Although in the flowchart, as shown above, the checkpoint in the incremental conductance algorithm is when the slope of the PV curve is equal to zero. But when implementing the algorithm, a practical approach is to let the gradient of PV

curve tend to some error value. In other words, the sum of the incremental conductance and the instantaneous conductance is set to a small error value at every operating point, given by $V\Delta I/\Delta V + I = e_p$ [6].

As the V_{ref} shifts towards V_{MPP} this error value, e_p tends to zero. The instantaneous values of PV voltage and current can be assessed by the voltage and current sensors connected strategically in the module converter. Once these values are registered by these sensors, a DSP or any microcontroller can work on them to calculate the incremental conductance algorithm.

The incremental conductance algorithm has its own share of issues though. It tends to have higher computational rate and lower sampling rate of sensed PV voltage and current [10]. But these issues can be ironed out by using a fast micro controller system.

2.4 Distributed MPPT

The advantages of distributed MPPT over the conventional MPPT are highlighted during partial shading and other mismatch issues. The d-MPPT in a module integrated converter realizes the local MPPT of each module unlike the conventional string MPPT. This leads to a increase in system efficiency. The d-MPPT renders more flexibility during the designing of a modular PV system and reduces the time for PV module placement in complicated rooftop architecture. With the engineering complications reduced with d-MPPT, a lower levelized cost of energy

(LCOE) and reduction in balance of systems (BOS) wiring cost can be achieved [15]. The maintenance of each PV module by implementing the d-MPPT is further streamlined. The overall lifetime of the system increases with the implementation of d-MPPT and makes the system easily replicable.

d-MPPT at PV sub-module level

In this thesis, the d-MPPT has been implemented at the PV sub-module level. A PV panel with 72 cells has been segmented into 3 sub-modules, each of 24 cells. With each cell having an open circuit (OC) voltage of 0.6 V, the OC voltage of a single module can be calculated as 14.4 V each. The short circuit current (SC) of each cell connected in series is taken from the SIM-ELCETRONICS model of a PV cell. The SC current of each cell is 7.34 A. With the rating of the module as 250 W, the power output yield of each sub-module at G = 1 (at maximum irradiance 1000W/m^2) is 85W. The d-MPPT operating on a sub-module with the change in irradiance from G = 1 to G = 0.5 is shown in Figure 2.9.

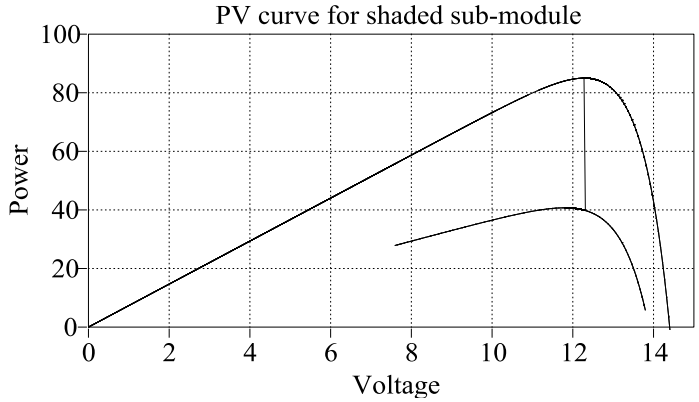

Figure 2.9 Distributed-MPPT in a PV panel for G =1 to G = 0.5

Chapter 3. Module Integrated Converters

3.1 Objectives of a Module Integrated Converter

In a conventional PV module-grid integration, many PV modules are connected in series. This string of PV modules is connected to a central dc-dc converter. The dc-ac inverter carries out the inversion process on the dc-dc converter output and finally connects the string PV module to the grid. Figure 3.1 gives a representation of this configuration.

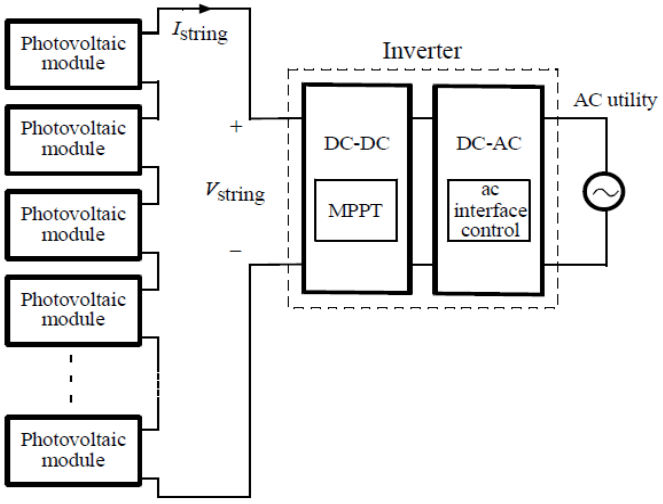

Figure 3.1 Conventional PV module string connection to ac grid [5]

Although this system is practical and is easy to implement, it has some major drawbacks. In systems with centralized dc-dc conversion, whenever the performance of even one module is impaired, there is a power loss along the entire PV array. Partial shading, soiling and aging related mismatches together with irregular maintenance make significant reduction in the system power output.

The power loss, especially in a residential system where there is a constraint on the number of PV modules, is not acceptable. The module integrated converter (MIC) can help overcome these challenges. In a MIC configuration a distributed modular architecture is prevalent. Each PV module is connected to an individual dc-dc converter with its own maximum power point tracking (MPPT) unit. In this way the power output of each module is maximized regardless of the performance of other modules connected in the same PV array. Figure 3.2 shows a MIC configuration.

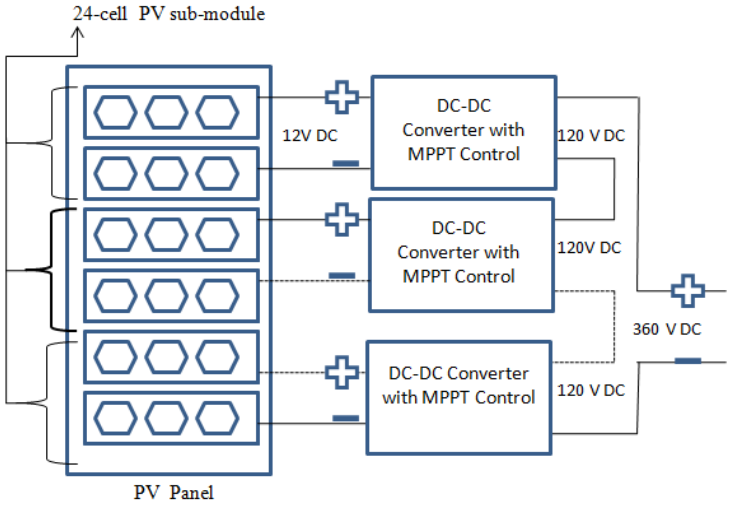

Figure 3.2 PV sub-module integrated converter configuration

This entire system enables the sub-modules to operate independently at their optimum power output level irrespective of the changes in the irradiance in each module. This effectively decouples the PV sub-modules from the rest of the system and eliminates mismatch losses. To increase the performance and level of in-

tegration and to decrease manufacturing costs, the DC-DC converter can be optimized for the particular PV sub-module and integrated directly on its back side.

3.2 DC-DC converter topologies for MIC

The PV MIC system offers ‘plug and play’ model. It greatly optimizes the energy yield for a single PV module. In the PV MIC system, the PV module produces low-varying dc voltage in the range of 20 - 40 V, depending on the number of cells in the module. Therefore, a high step-up (5X) dc-dc converter topology, which has a high conversion efficiency, small size and high voltage conversion ratio, is needed for a practical PV MIC system.

Switched Capacitor Topology

In MIC configurations, there has been a lot of research on panel level dc-dc converter solution which can be inserted into a chip with embedded control, sensing technology, low power consumption and takes up less space.

For a board level solution for PV module integrated converter inductor-less topologies, devoid of large magnetic components, need serious consideration. These inductor-less topologies are prevalent in power supplies for computer processors. They work at 10X level of dc-dc conversion ratios, making them attractive proposition for the module level converters for residential photovoltaic systems.

Many traditional dc-dc converters have been proposed to step up the voltage for the PV module connected in string. All these topologies suffer one serious de-

sign drawback. Most of these topologies have either inductor based topologies or employ resonant switching strategies for soft switching purposes, which again introduce inductors in the circuit. These inductors in the converter make the cost and design of the circuit sub-optimal.

The motivation for the Switched Capacitor (SC) topology can be drawn from the various computer processor applications operating at low voltages in the range of 1.2 – 2 V. They require dc-dc converters which can step down voltages from 12 V to 1 V operating at high conversion ratios. Switched-capacitor (SC) and other charge pumps topologies convert the bus dc voltage to the level required by these processor applications. The absence of large magnetic devices like inductors or high frequency transformers, as needed in the power circuit of conventional dc-dc converters, increases the possibilities of IC fabrication of these topologies [10]. Using basic SC cells in filter designs, numerous switching techniques have been proposed for dc-dc power conversion. The switched capacitor topology used in dc-dc converter for PV module need to replicate the boost design but without the inductors or other magnetic device.

But like every dc-dc conversion design, switched capacitor converters also have a few negative aspects which need attention [10]:

- Weak regulation capability
- Voltage conversion ratio, which is structurally determined by the circuit topology

- Pulsating input current that introduces electromagnetic interference (EMI) with the supply network and other circuits
- Unidirectional power conversion

The first three negative issues associated with switched capacitors can be tackled by applying the current control scheme, voltage step-down and step-up converters. These schemes have been proposed in various literatures for further analysis. They feature improved regulation capability and continuous input current. The voltage conversion ratio is determined by a control voltage that adjusts the charging trajectory of the capacitor. However, regarding the last negative aspect against the switched capacitor circuit, apart from the converters with magnetic components, articles investigating IC-based switched capacitor bi-directional converters are fewer in number [10].

The benefits of Switched Capacitor Topology

As underlined earlier, switched capacitor converters help achieve current and voltage conversion without the use of any magnetic energy storage device. In Figure 3.3 the cost and volume per energy storage (μJ) for a sample of discrete capacitors and inductors usable in power applications are shown.

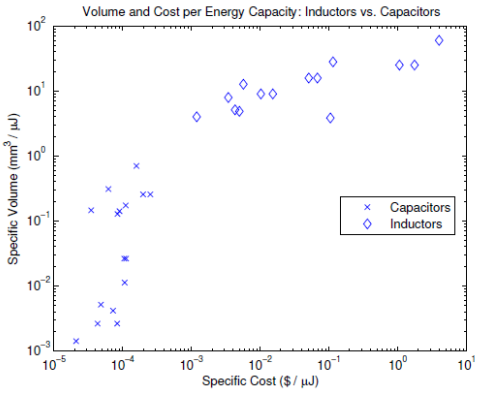

Figure 3.3 Specific cost and volume comparison for capacitors and inductors [9].

These data in the figure imply expected cost and volume benefits of switched capacitor converters when compared to inductor-based converters.

Marx Multilevel Converter

One particular realization of the switched capacitor MICs for the PV module application as given in Figure 3.4 is the Marx Multilevel converter [9].

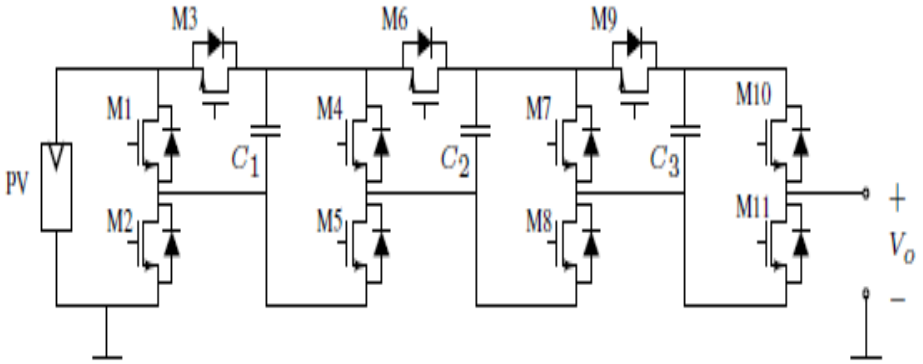

Figure 3.4 Marx multilevel converter [9]

With series and parallel combinations of the input source and the switched capacitors, the 5-level Marx converter shown in Figure 3.4 achieves integral con-

version ratios given as $Q_{avail} = [0, 1, 2, 3, 4]$. This conversion ratio array shows the maximum capability of the particular converter where the conversion ratio can be as high as four times the input voltage source. Moreover this array also points out the flexibility that can be achieved in the conversion ratio [9].

The switching cycles for these multilevel converters can be broadly categorized into two phases: Recharge phase and the output phase. During the recharge phase, the connection between the switched capacitors and the load is severed with capacitors getting charged to the same equal voltage while in parallel connection with the input source. During the output phase, at least one of the several series-parallel configurations of the switched capacitors and input source can be chosen for the desired conversion ratio [9]. There are many redundant switching configurations possible in this scheme. Typically, the switching configurations are chosen such that number of switches in the circuit path connecting the output and the voltage drop across the capacitors is kept at a minimum. This scheme helps in maintaining the load regulation. The rules of thumb to minimize capacitor droop include driving the output with the input source connected and utilize all of the switched capacitors during the output phase. That implies that whenever possible also connect the redundant capacitors [9].

Widespread grid penetration of PV will rely on the reduction of capital cost and total cost of ownership for solar power systems. It is critical that these factors guide the design of photovoltaic power circuits and system architectures. This

work has presented a full system approach utilizing switched capacitor multilevel DC-DC converters. Substantial cost reductions may be possible by providing per panel MPPT without the need for per panel magnetic.

Extended boost converter

In this thesis the focus has been to boost the dc voltage of input source of the PV module to large value. Since the idea is to string the dc converters together to form the series array, the value of the output voltage plays a significant role. The regulation of the output voltage of the PV string is essential as this voltage is then fed to the dc-ac interconnection. The large conversion ratios (e.g.1.2V/12V = 10) of conventional multiphase converters pose significant design challenges at high switching frequencies (e.g. > 500 kHz), requiring a high PWM resolution for tight voltage regulation [7]. This idea of the extended duty ratio converters usable in PV module converters can be traced to the voltage regulator modules which need high current output with steep slew rate. The modification in this idea is to utilize this converter for stepping purpose without driving the duty ratio to upper saturation limit. The current unbalance between the two input inductors (in case of boost configuration) can be removed without any addition of current sensing technique.

Large conversion ratios create asymmetrical unloading and loading current transients. Large transients are created during unloading step changes since the steady state duty ratio is close to the upward saturation limit. The line transient

response is determined by the current slew rate of the input filter. The control bandwidth decided the slew rate when the duty ratio nears saturation [7]. It is also inversely related to the size of the input inductor during duty ratio saturation. The transient response might improve by reducing the inductor size but it ends up with larger input capacitor to maintain the same input voltage ripple specification.

The points where the extended duty ratio converter scores over the multilevel conventional converters apart from the usual stepping up capabilities at lower value of duty ratio are the inherent ripple cancellation of the respective inductor currents, smaller design of the input ripple LC filter and dynamic response which is faster than the conventional multiphase converters [7]. Since the current balancing of inductor current is a trait of the extended duty ratio converter, the high cost and precision of the current sensing techniques can be avoided in the main circuit.

The main difference between the extended duty ratio converter and the conventional multiphase converters is the addition of the capacitor, C1. The additional capacitor not only reduces the voltage across the switch to half its conventional switch off voltage value but also helps in balancing the inductor current in both the phase without the addition of any current sensing circuit. It has been shown in literature that with identical components for different phases and novel modifications in control, the dynamics introduced by the capacitors do not alter the design of the controller considerably. The voltage or current controller designs used in case of the conventional converters can also be used for extended duty ratio converters.

Steady State Analysis

The extended duty ratio converter is shown in the Figure 3.5.

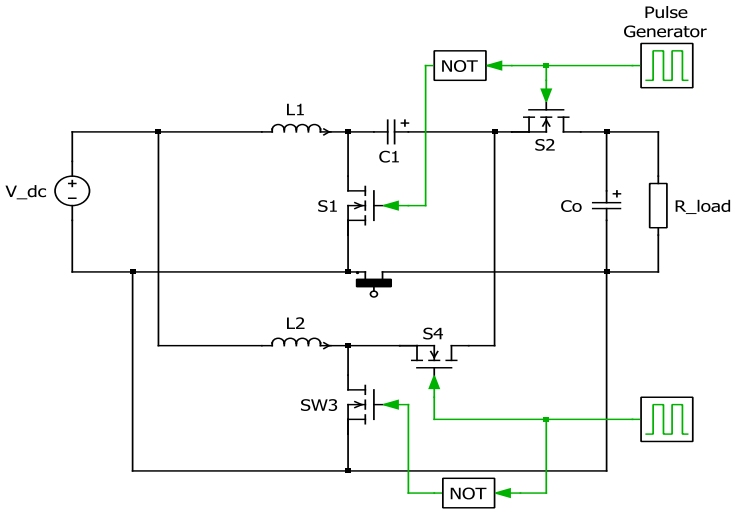

Figure 3.5 Two phase extended duty ratio boost converter

The converter can also be identified as step-up two phase boost converter. It bears a close resemblance to the conventional synchronous boost converter with the only change being the addition of the energy storage converter C1 in the upper phase between inductor L1 and the switch S2. Each phase has a main switch and the synchronous rectifier switch. In the figure the S1 and S3 are the main switches and the S2 and S4 are the rectifier switches. The input terminal which in this case would be the output nodes of the PV module is connected to the two inductors L1 and L2 while the output terminal of the lower phase is connected between the capacitor C1 and synchronous rectifier switch S2. The main switches in both the phases S1 and S3 are switched at 180 degree phase shift. The working duty ratio, D of the entire converter has to be kept at more than 0.5 in value [7]. In this thesis the duty ratio is kept at 0.8 in steady state in order to attain conversion of 10X. In

a conventional boost converter the duty ratio will be at 0.9 for the same conversion pushing the value of d to close to the upper saturation limit.

During the state 1 of the operation as shown in the Figure 3.6 both the main switches S1 and S3 are turned on with switches S2 and S4 turned off.

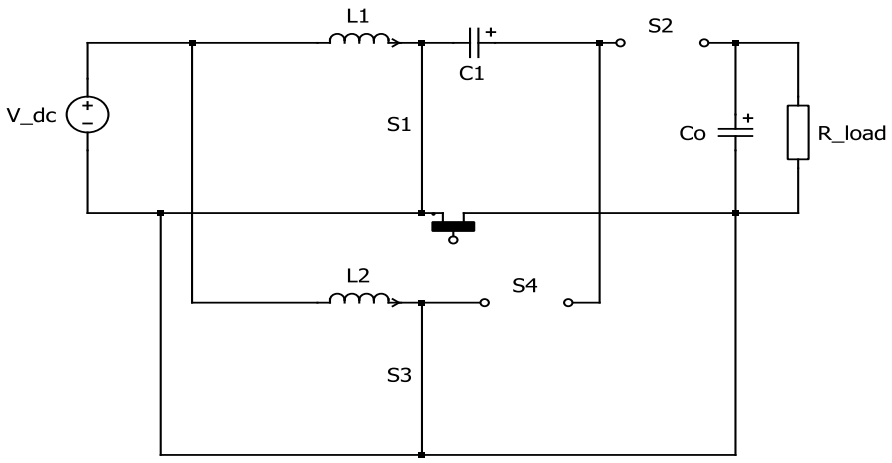

Figure 3.6 Extended duty ratio circuit during state 1 operation

During this phase of operation the input circuit consists of the input voltage source (the output node of the PV module) and the two input inductors L1 and L2. Accordingly, the input energy is equally stored in the inductors during this charging mode with the inductor currents I_{L1} and I_{L2} increases linearly. The rate of increase of these currents is determined by the value of the input source voltage ($V_{dc} = E_i$), the value of the inductors L1 (or L2) and the switch on time, DT_s. Analyzing the voltage during state 1 analysis across L1 and L2:

$$V_{L1} = V_{L2} = V_{dc} \tag{3.1}$$

During state 2 of this circuit operation as shown in Figure 3.7 below the main switch S1 continues to be in the ON state while the main switch S3 is turned OFF.

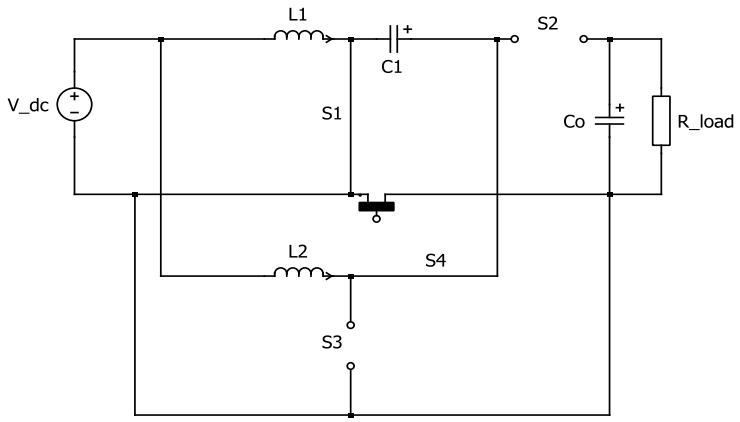

Figure 3.7 Extended duty ratio circuit during state 2 operation

The inductor current I_{L1} continues to rise with the same slope with inductor L1 in the charging mode. Inductor L2 enters in a discharging mode with the synchronous switch S4 turned on. The discharging route of inductor L2 consists of the input source V_{dc} and the energy storage capacitor C1 and the switch S1. The rate of decrease of the inductor current I_{L2} is decided by the steady state voltage of the storage capacitor C1, input source voltage V_{dc} and the turn off time of the main switch given by $(1\text{-}D)T_s$ where T_s is given by the switching time period (T_s=1/switching frequency, f_s). Analyzing the voltage during state 2 across L1 and L2:

$$V_{L1} = V_{dc} \tag{3.2}$$

$$V_{L2} = (V_o / 2) - V_{dc} = V_{C1} - V_{dc} \tag{3.3}$$

The state 3 of the circuit analysis is a repeat of the switching configuration as mentioned in state 1 and shown in figure 3.6. Hence, the switches S1 and S3 are in ON state with the synchronous switches S2 and S4 turned OFF. Both the inductors enter the charging mode [7].

The state 4 and the final stage of operation of this converter can be seen as the reciprocal of the state 2 of the circuit steady state operation.

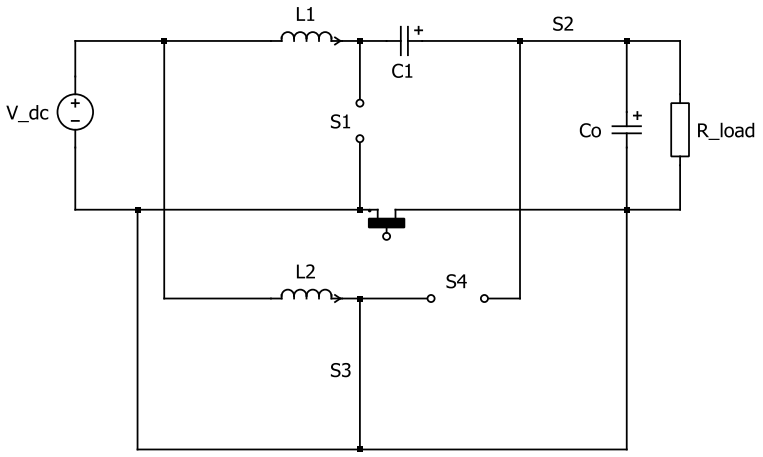

Figure 3.8 Extended duty ratio circuit during state 4 operation

This is shown in Figure 3.8. In this state L1 enters discharging mode with the inductor L1 discharges its stored energy through the circuit path including the input voltage source V_{dc}, the storage capacitor C1, and the switched on synchronous switch S2. The rate of discharge or rate of change of current through L1 is given by the difference between the output voltage V_o and the sum of steady state capacitor voltage V_{C1} and input voltage V_{dc}. The inductor L2 undergoes the charging mode with the inductor current I_{L2} increases linearly with time. Analysing the voltages across L1 and L2 during state 4 of operation:

$$V_{L1} = (V_o / 2) - V_{dc} = V_O - V_{C1} - V_{dc} \quad (3.4)$$

$$V_{L2} = V_{dc} \quad (3.5)$$

The ratio between the input voltage (the output voltage of a PV sub-module) and the output voltage of the converter can be calculated using the voltage second balance across the inductors L1 and L2 over T_s.

$V_{C1}(1-D) = V_O(1-D) - V_{dc}$ ….Voltage-sec balance across L1

$V_{dc} = V_{C1}(1-D)$ ….Voltage-sec balance across L2

$$\frac{V_{dc}}{V_O} = \frac{2}{1-D} \quad (3.6)$$

The steady state voltage across the storage capacitor C1 can also be calculated using the above stated equations. The voltage across C1 is given by:

$$V_{C1} = \frac{V_{dc}}{1-D} = \frac{V_O}{2} \quad (3.7)$$

The Extended-D converter has a natural mechanism to balance the average inductor currents within this 2-block system. The steady state amp-second balance of the storage capacitors forces the average inductor currents to be equal, if a common duty ratio is used [7]. The capacitor acts as the source for the inductor current I_{L1} during $(1-D)T_s$ while it behaves as sink for the inductor current I_{L2} during the state 2 of the steady state operation of the extended duty ratio boost converter.

Chapter 4. Analysis of Single Panel Module Integrated Converter

The previous chapters provided an insight into the development and analysis of various topologies for the dc-dc converter for the PV modules. The aim in this chapter is to identify a converter topology which can extract the maximum output power from sub-modules connected in a series string inside a PV module, in an efficient manner. While some topologies have certain design issues others have efficiency issues, the fact is they all have some drawbacks which need to be perfected. The aim of discussing this issue is to use a particular topology that can be best optimized for providing the boost in the PV output voltage. The string voltage of the entire array needs to be regulated for all operating conditions.

A photovoltaic series connection consists of various PV modules connected in series. These series connections are connected in parallel to make the PV array. Although the PV modules are considered homogeneous packages of PV cells, it is possible, to an extent, that the manufacturing composition of the PV cells vary inside a module.

Such cases are rare as the manufacturing of these modules are highly regulated with enough precautions being taken to maintain high manufacturing standards. The sub-module converters play an important role during any instances of partial shading on these modules.

4.1 Series connected PV sub-module

With the concept of the d-MPPT at the sub-module level introduced in the previous section, this section will concentrate on the series connection of the PV sub-modules inside a panel. The PV sub-modules, designed using PLECS simulation tool, takes into account the open circuit voltage and the short circuit current of each cell in the sub-module. The idea is to design a dc-dc converter prototype which can substitute the bypass diodes and act on the sub-module voltage.

During the simulation of partial shading using PLECS, the irradiance level G, of each sub-module can be changed at any time instant. The PV sub- module voltage with G=1 stays constant at around 12.28 V, the sub-module V_{MPP}. The PV voltage of the sub-module with change in irradiance, changes according to the d-MPPT incremental conductance algorithm. Figure 4.1 shows the change in PV voltage of the sub-module with respect to the V_{ref} generated by the d-MPPT controller.

It is evident in the Figure 4.1 that V_{pv} consistently tracks V_{ref} signal generated by the d-MPPT Incremental conductance algorithm. The irradiance level of the partially shaded sub-module is changed from G = 1 to G = 0.5 at t = 0.2 s from the start of simulation. The V_{pv} plot (in red) follows the V_{ref} (in green) with increase in time until it settles at the new V_{MPP} value for G=0.5 which is 11.8 V. The V_{pv}

reaches the new V_{MPP} at approximately t=0.5 s and then finally settles into the 'stable point'.

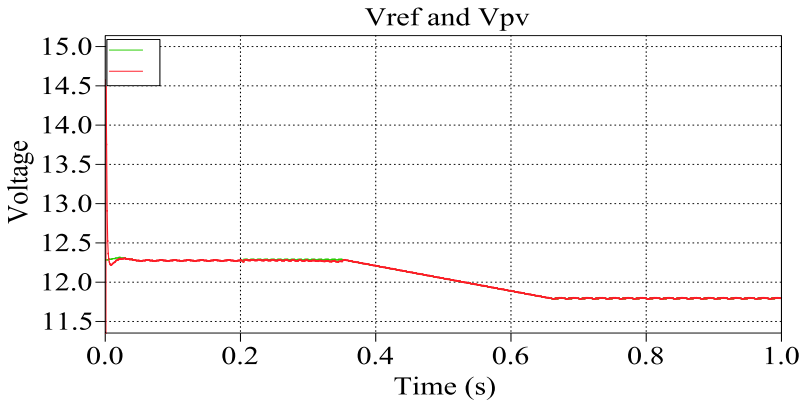

Figure 4.1(a) V_{pv} and V_{ref} in the partially shaded sub-module

4.2 DC-DC boost converter power stage design

While all the topologies discussed till now have their own advantages and disadvantages, the purpose of experimenting with different topologies remains the same, i.e. to regulate the dc interconnection voltage for all values of irradiance. In this thesis the boost topology is selected for the sub-module integrated converter. Although the extended duty ratio boost converter topology was experimented with initially, finally the boost topology was chosen for the dc-dc converter in this particular context for simulation and hardware prototyping.

The topology of the dc-dc converter has been designed to boost the PV voltage from 12 V to 60 V (nominal) for each sub-module in normal operating condition. The three sub-modules connected in series lead to a total dc interconnection voltage of 180 V when there is no partial shading.

During the partial shading, simulated for a single sub-module connected to the micro-inverter, the dc interconnection voltage is still maintained at 180 V, even though there are changes in the individual voltage contribution of each sub-module. The output voltage of the sub-module subjected to partial shading drop from the nominal voltage of 60 V to values corresponding to its irradiance level, with appropriate changes in the value of the duty ratio decided by the input voltage controller. The output of the sub-modules subjected to normal level of irradiance, G = 1 changes compensating for the drop in the output voltage of the partially shaded sub-module. Figure 4.2 shows the sub-module output voltages during irradiance change from G=1 to G=0.5.

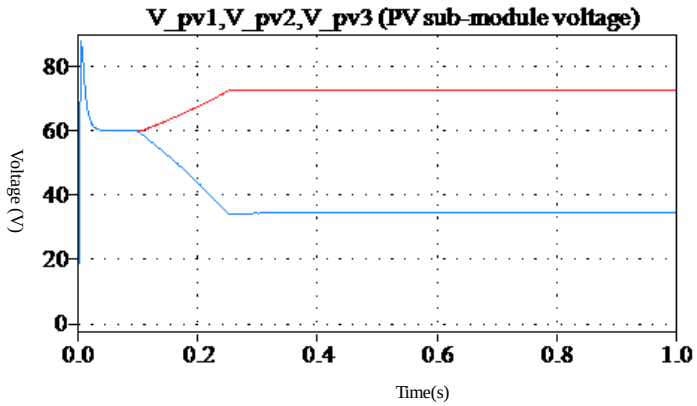

Figure 4.2 Sub-module boost output voltages for irradiance change G=1 to 0.5.

For the change in irradiance from G =1 to G = 0.5, the input inductor current for the boost converter also undergoes change. The inductor current for the sub-modules with G = 1 remains the same for any change in irradiance in other sub-

module. Figure 4.3 shows the inductor current switching waveform of the sub-modules with nominal irradiance. Figure 4.4 shows the switching waveform along with the change in PV current for the partially shaded sub-module.

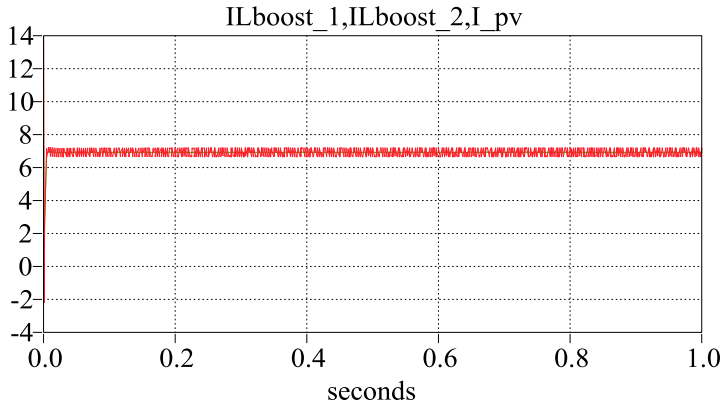

Figure 4.3 Inductor current and the PV current in un-shaded PV sub-module.

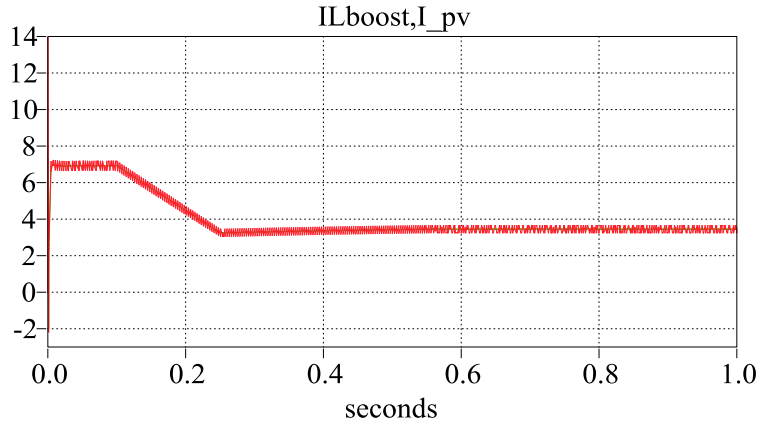

Figure 4.4 Inductor current and the PV current during partial shading.

In the simulation, the partial shading conditions are incorporated gradually at t = 0.1 s. The value of the irradiance is changed from G = 1 to G =0.5. Irradiance value changes from G = 1 at 0.1 s and settles at G = 0.5 at t = 0.25 s.

Basics rules of steady state dc-dc converter topology design were adhered to while designing the power stage of the boost converter for the PV sub-modules. The calculations carried out in the design are given below:

$$L = \frac{V_O D(1-D)}{\Delta I_L f_s} \quad = 40\mu H \tag{4.1}$$

$$C_O = \frac{I_o D}{\Delta V_O f_s} \tag{4.2}$$

The power stage of the dc-dc boost converter in connection with the boost converter is given in Figure 4.5**.** The figure depicts the PV sub-modules with and without partial shading, the dc interconnection link and the d-MPPT blocks.

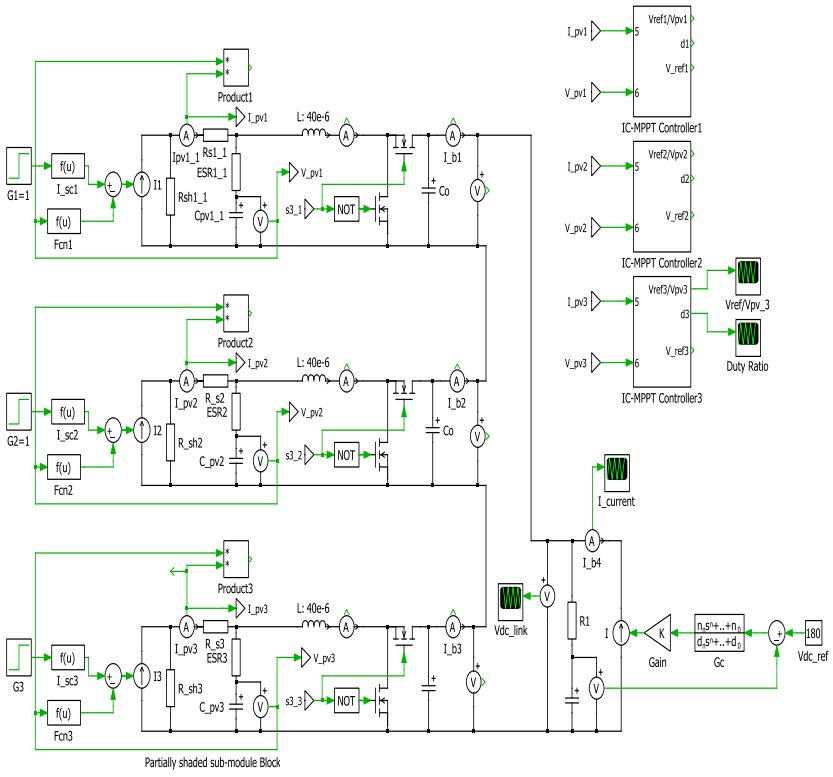

Figure 4.5 PV Sub-module with boost converter and MPPT controller

The values of L and C are calculated for switching frequency, f_s = 500 kHz. The value of L is calculated at D = 0.5, which is the worst case condition (maximum inductor current ripple) for a boost converter. The value of the output capacitor is calculated taking into cognizance the capacitor R.M.S. current. The value of the capacitor $C_O = 20\mu F$ is calculated under this consideration.

4.3 Input PV voltage controller design

The input voltage controller of the PV sub-module plays a critical role. The controller is modelled on the lines of an output voltage controller of any buck converter. Using the duality of the buck and boost converter design, this controller can be used to control the input PV voltage of the boost converter. The voltage controller is determined by the K-factor method [7]. It is based on the input voltage to duty ratio transfer function. The major change in the controller formula is the substitution of the term R_{Load} used in the conventional controller with R_{pv}, the effective input load resistance for the boost converter. The value of the R_{pv} is calculated by finding the ratio of the V_{MPP} with I_{MPP} at G = 0.1 irradiance. This assumption holds given that the ratio of the V_{MPP} and I_{MPP} does not change drastically with irradiance for a sub-module around the various MPP points. The value of V_{MPP} varies from 12.28 V for G=1 to 11.34 V for G = 0.2 irradiance level. The input voltage to duty ratio transfer function is given by

$$\frac{\tilde{v}_{pv}}{\tilde{d}} = \frac{V_O(1 + C_{PV}R_{esr})}{1 + s\left(\frac{L}{R_{PV}} + C_{PV}R_{esr}\right) + s^2LC_{PV}(1 + \frac{R_{esr}}{R_{PV}})} \tag{4.3}$$

Using the K factor method, a type II controller is designed with a bandwidth of 1 kHz and phase margin of 60 Hz for this input transfer function. After deciding the bandwidth, the type II controller function is calculated as:

$$G_C(s) = \begin{cases} \dfrac{(s + w_z)w_z}{s(s + w_p)w_p} \\ \dfrac{117.32(s + 5189.41)}{s(s + 7610.35)} \end{cases} \tag{4.4}$$

Figure 4.1 represents the action of the input voltage controller. The controller dynamics is correct as the value of V_{pv} changes with V_{ref} for any change in irradiance in one of the sub-modules. Although the transients in voltage V_{pv} is considerable at the instant when the change in irradiance takes place, this can be neglected as it stretches only for a few micro seconds in time.

4.4 DC Link stage design

The DC link stage design is another crucial segment of the entire converter design. This stage is designed to mimic the interconnection between the sub-module dc-dc converters connected in series and the ac grid or in terms of the residential PV system, with the micro-inverter. The dc link interconnection consists of a controller which tracks the dc link reference voltage which needs to be maintained at 180 V by changing the current source that simulate the inverter. This controller commands the current source to the right value needed to regulate to 180 V. In steady state this will exactly equal I_{STRING} decided by the MPPT of

the individual sub-modules. This helps in maintaining the regulation of dc link voltage of the interconnection. As is evident in the Figure 4.5, the voltage across the PV sub-module string connection stays at 180 V regulated even when one sub-module experiences change in its direct irradiance, G. In other words, it eliminates another dc-dc converter at the string interconnection. This modification can act crucial in the residential PV installation where the installation and maintenance cost margins are always under pressure. The dc link stage behaves more like a simulation of a micro-inverter at the interconnection. The dc link compensator stage is defined with respect to the transfer function which includes the dc link impedance and the current source. Figure 4.6 best describes the dc link stage along with the controller.

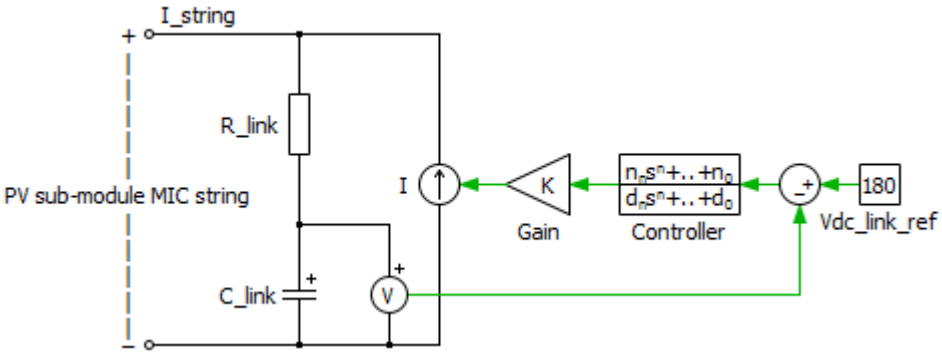

Figure 4.6 DC link stage compensator

4.5 DC link stage transfer function

The PV sub-module MIC string has been shown and explained in detail in the previous sections. The transfer function representing the dc link interconnection

deals with the input impedance, in this case the series connection of R_{link} and C_{link} with the assumption that the I_{STRING} is determined only by the MICs and their MPPT implementation and is not affection by the dc link voltage controller. The transfer function can be defined as:

$$T(s) = Z(s) = \frac{1 + R_{link}\, C_{link}\, s}{C_{link}\, s} \tag{4.5}$$

The values of C_{link} and R_{link} used in the simulation and in the controller design are 20 μH and 1Ω respectively.

4.6 Controller design of the dc link stage

The controller design for the dc link stage for the PV sub-module system as discussed in this thesis is based on the K-factor method. The transfer function of this dc link interconnection has been dealt with in the previous paragraph. The K-factor method used for the controller design gives the following result

$$G_C(s) = \frac{K(s + 173.09)}{s(s + 2280.79)} \tag{4.6}$$

This is a much slower controller compared to the input voltage controller designed for the d-MPPT algorithm. The bandwidth of this controller is kept at 100 Hz and the gain *K* in the formula is given by 28.79. The change in the irradiance incident on one sub-module is a slow process involving the erratic movement of cloud cover. The series string current I_{STRING} changes only when the irradiance on

a particular sub-module changes. The issue of voltage regulation across the PV sub-module string dc interconnection is important during this time. This regulation capability has been shown earlier in Figure 4.4 for a change in irradiance in one sub-module from G = 1 to G = 0.5.Once the system reaches the MPP, the compensator circuit will view the PV sub-module side like an open circuit connection. Thus a slower controller can actually serve the voltage regulation purpose. Figure 4.7, Figure 4.8 and Figure 4.9 show the system simulations when the irradiance changes from G=1 to G=0.8 for a sub-module in the same PV system.

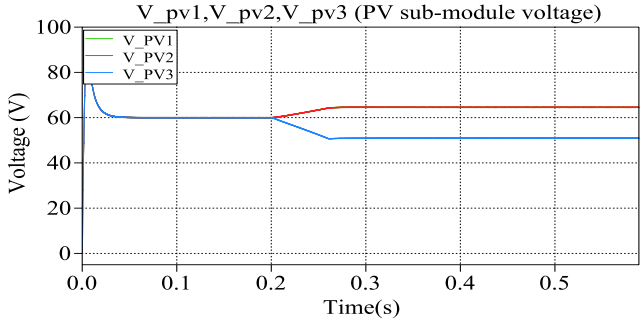

Figure 4.7 PV sub-module individual voltage for G=1 to G=0.8

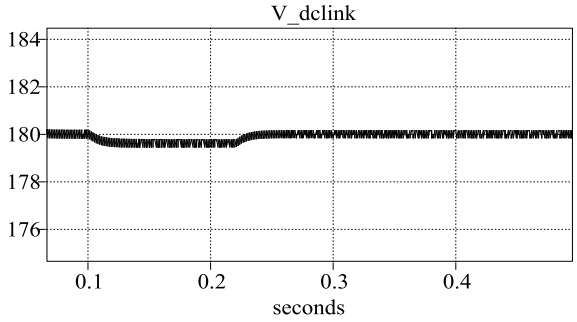

Figure 4.8 Net PV module voltage at dc link. Change in irradiance, G at t = 0.1 s with net voltage regulated at 180 V.

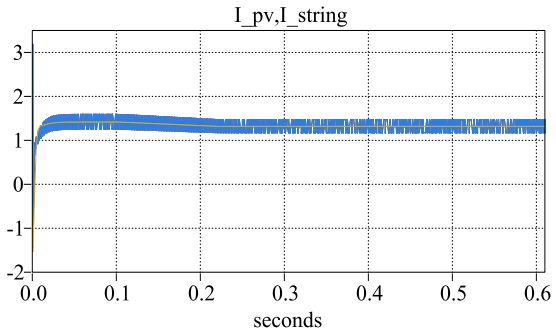

Figure 4.9 I_{STRING} current and I_{PV_SERIES} current for G = 1 to G = 0.8.

Chapter 5. Multiple MIC Analysis

5.1 Module integrated converters analysis

The centralized PV array systems have made huge development over the last decade but it has yet to make definite incursions into the conventional energy sources. To increase the popularity of the PV system, the residential PV systems needs more technology impetus. Rooftop PV systems are attracting major attention as it nullifies the need for large open space, which is a pre-condition for the centralized large PV array field. It also empowers the consumers to control their own home energy demands. This is where the module integrated PV converters assume an important role.

Module integrated converters (MIC) essentially make the PV 'plug and play' model possible. Any MIC typically consists of a dc-dc converter followed by centralized dc-ac inverter grid system or another dc-dc converter for stand-alone residential system [7]. All the MICs are powered with autonomous control to counter the partial shading conditions by implementing a type of distributed maximum point tracking algorithm.

MICs are an integral part of a PV module. A MIC is able to unlock the maximum output power by employing the MPPT in every panel. In a conventional centralized string converter, the power loss due to partial shading on a group of modules in an entire string is high leading to poor efficiency. Such low levels of efficiency cannot be tolerated in residential PV system. In addition to this prob-

lem, there is also the conversion loss in the central dc-dc converter or the dc-ac inverter which must be considered when the conventional centralized string converter design is considered.

The MIC design also helps in countering the hot-spot conditions in each panel which arises during partial shading. Since the MICs are operational at the panel level, it removes the need for a bypass diode across the panel.

5.2 Series connected MICs

The dc-dc MIC can be categorized into two types. One is the series connected module integrated converters and the other parallel connected to the dc link. Figure 5.1 show a typical series connected MICs.

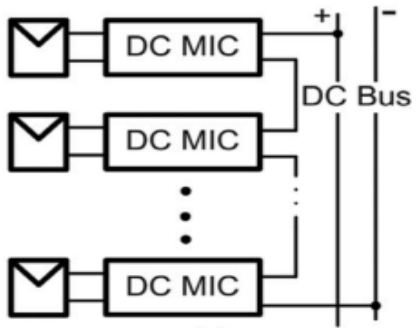

Figure 5.1 Series connected MICs [8]

While the parallel connected MICs are left for later discussion in this chapter, this section will concentrate on the series connection of the MICs. In the series connected MICs, as is evident from the Figure 5.1, there is a clear scope of implementation of panel level MPPT. The series connection of MICs allows in building a high voltage across the entire series which can be interconnected to the

dc link. This configuration is perfectly helpful in large systems where the dc input of the dc-ac inverter is in the range of 360 V or above. Since the dc link voltage can actually be built up by adding MICs in series, there is less pressure on the conversion ratio of the MIC converter. Hence simple non-isolated dc-dc converter topologies can be used in these MICs [9].

This system has its own share of drawbacks. Since the modules are series connected, it renders a level of inflexibility during the cases of extreme partial shading. If any of the MICs fails to function or gets disconnected, this series configuration will face problems. In order to maintain the series current, there still needs to be a path for the current to flow during the case of a failed MIC.

In this research project the concept of series connected MICs has been analyzed at PV sub-module level. The localization of the MICs at the sub-module level helps in building up the output voltage from each panel. With the series connection of these MICs, the net string-dc interlink voltage can be increased. The constraint on the number of PV panels being connected in series to attain a particular level of conversion can be lessened.

In the Figure 5.2 the sub-module level localized MIC is shown. The block representing the PV module actually consists of the PV sub-modules and the boost converter combination, introduced in chapter 4. Figure 4.5 gives a complete picture of the composition of this block. This connection has been analyzed with another PV module block in series. In this simulation setup, the net conversion

ratio from the sub-module level to the dc link stage is from 12 V dc nominal to 360 V dc.

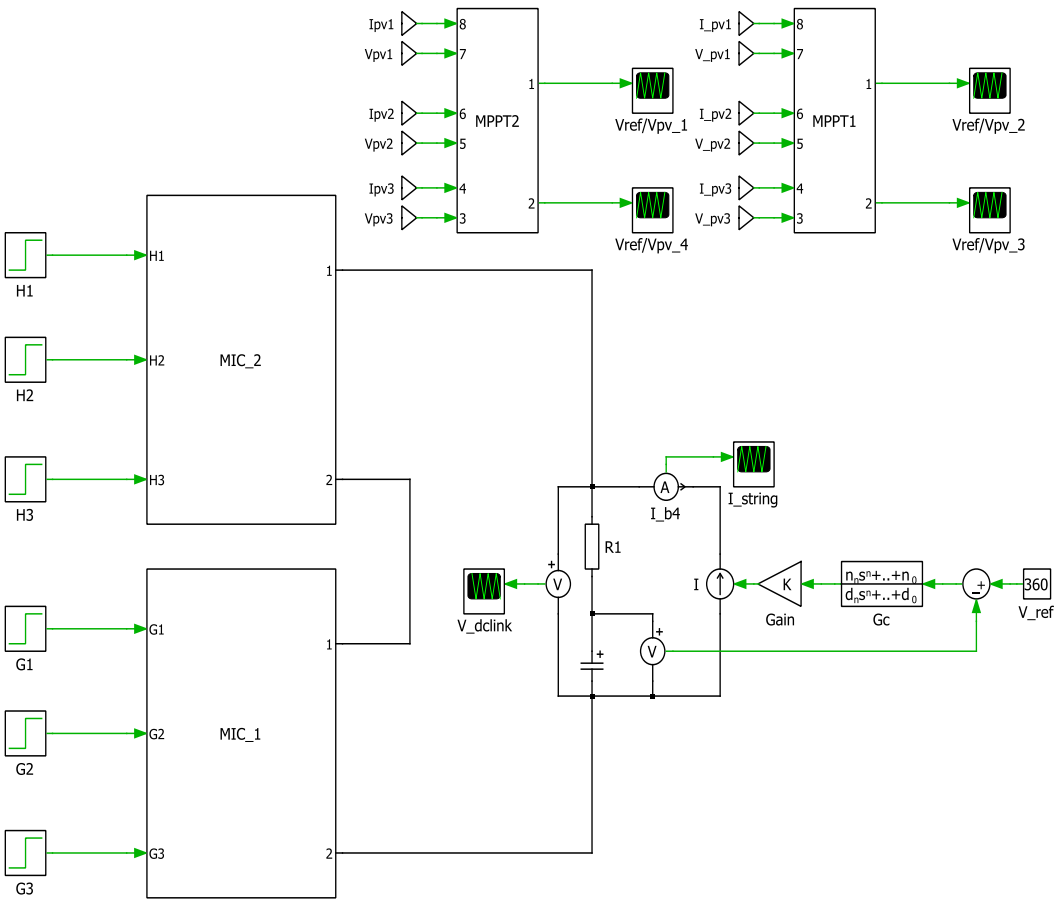

Figure 5.2 Series connected MICs in PLECS. The blocks H1, H2, H3 represent the irradiance level of another PV module.

Series connected MIC analysis

As represented in the Figure 5.2, the block MIC_2 represents the sub-module level integrated converter for another PV module. The two MICs are connected in series. Nominally, each MIC boosts the input voltage of the PV sub-modules from

12 V to 60 V. Two MICs connected in series create a dc link voltage of 360 V at normal values of irradiance (G = H =1). In this simulation, the irradiance of the PV sub-module (G_3) in MIC_1 is changed from G =1 to G = 0.8. Figure 5.3 show the change in $V_{PVsub\text{-}module}$ with respect to V_{REF} for the partially shaded sub-module in MIC_1.

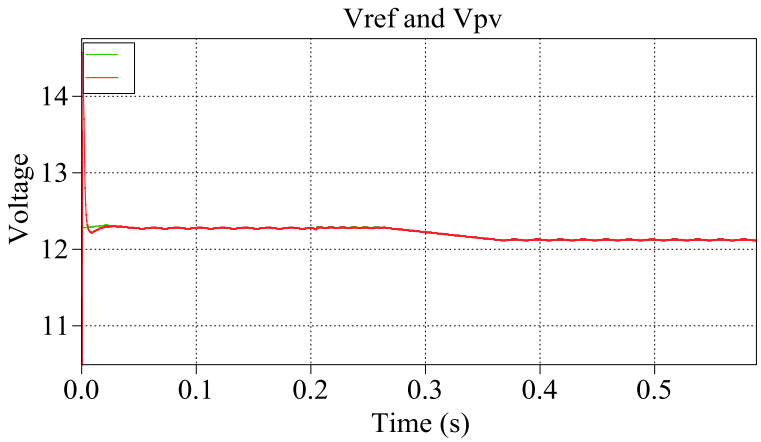

Figure 5.3 V_{REF} and V_{PV} in series MICs.

This change in irradiance is carried out instantaneously at t = 0.2 s. This assumption is valid since the sub-module consists of only 24 PV cells and the impact of spot-partial shading on this small area in the entire PV module will be instantaneous.

The PV MIC voltage can be analyzed in more detail. Figure 5.4a and Figure 5.4b represents the change in the PV MIC output voltage for each sub-module for a change in irradiance in one sub-module in the neighboring panel.

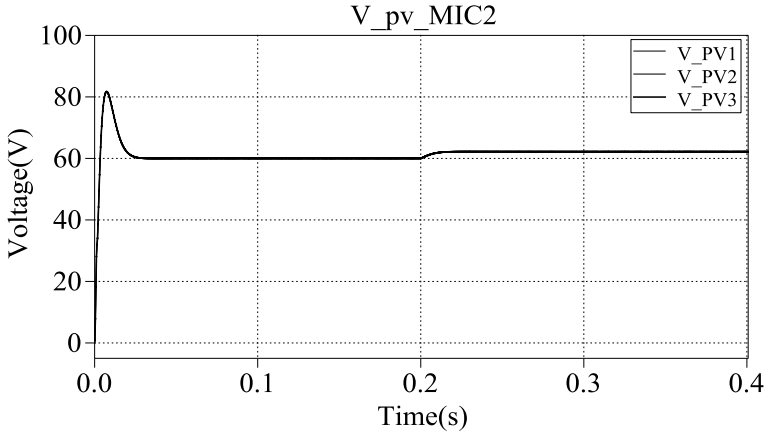

Figure 5.4 (a) PV MIC_2 output voltages for un-shaded panel.

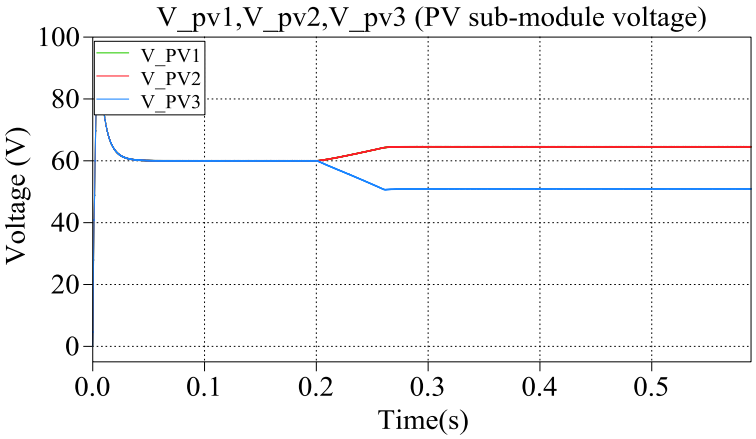

Figure 5.4 (b) PV MIC output voltages for the partially shaded panel MIC_1.

The total output voltage of the MIC_1 is 173.3 V after the change in irradiance. The individual voltages of the un-shaded modules in MIC_2 change from 60 V to 62 V with the change in irradiance in MIC_1. The total output voltage of the un-shaded MIC is 186.4 V. The output voltages in the partially shaded module MIC_1 changes such that the output voltage of the MIC series string remains regulated at 360 V. This voltage regulation at the dc link allows the removal of the dc-dc central converter for such a situation. The Figure 5.5 show the dc link regulated vol-

tage for the MIC series connection when the irradiance G_3, in MIC_1 changes to 50% of normal irradiance.

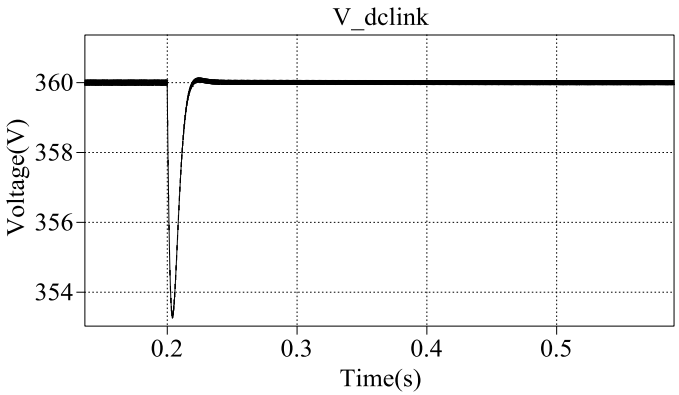

Figure 5.5 DC-link voltage for change in irradiance from G_3=1 to 0.5

The change in duty ratio of the un-shaded and shaded modules also needs a mention. Due to regulation constraint at the dc link, the duty ratio each boost converter self adjusts itself in order to output the desired MIC voltage. Figure 5.6a and Figure 5.6b show the change in duty ratio for the same irradiance change.

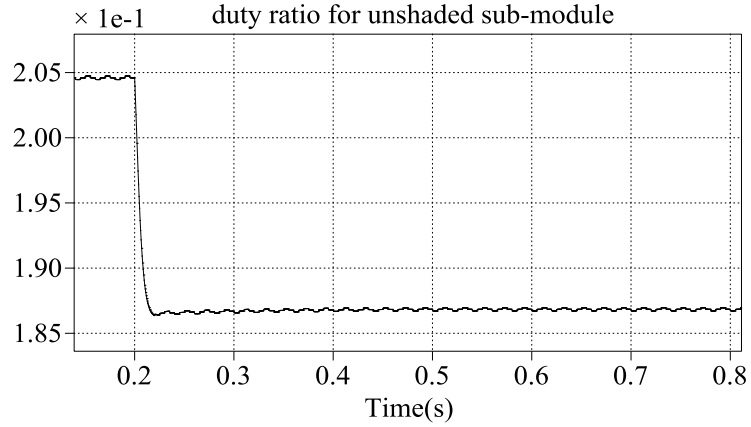

Figure 5.6 (a) Un-shaded MIC duty ratio

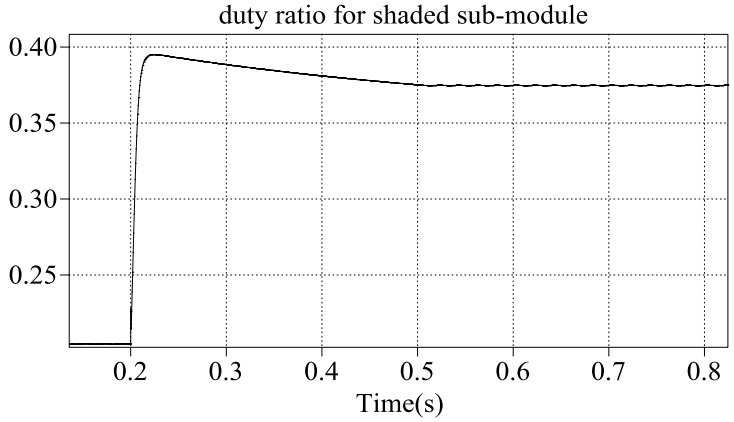

Figure 5.6 (b) partially shaded MIC duty ratio

The duty ratio of the un-shaded sub-module changes from D = 0.2 to D = 0.187 (buck configuration) approximately while the duty ratio of the shaded sub-module changes from D = 0.2 to D = 0.37 (buck configuration). The input voltage controller discussed in the previous chapter enables this change for the change in irradiance (G=1 to 0.5) and the corresponding change in the input voltage.

The input boost current of the MICs are same as the current waveforms discussed in the previous chapter. This is expected since the MIC connections are in series which is an extension of the sub-module architecture in a broader perspective.

Modified Flyback converter

As discussed in earlier section the series connection of the MICs can have some constraints. The number of MICs connected in series depends on the limitations of the dc bus voltage and conversion gain. Moreover if there is a case of extreme partial shading the MIC string voltage can be extremely low leading to sub-

optimal energy harvesting from the modules and loss of regulation at the dc link. In order to overcome this problem, a central dc-dc converter may be necessary in this situation. Since, each string may produce a different voltage based on shading and distributed MPPT, another dc-dc converter is needed in each string to regulate the output voltage to a common reference. Instead of using a dc-dc converter that produces 400 V it is simpler and more cost effective to use a dc-dc converter that produces a much lower voltage but connected in series with the output of the string. The new converter at its output handles the same current as the string and generates much lower voltage, and hence, its power rating and losses are significantly lower.

The control philosophy for this converter is to produce a voltage that is equal to the difference between the required reference voltage and the actual output of each string under any given operating condition. It turns out that for panels with MIC this feature is not needed, but for series connected strings of panels with no MIC, this is a good option. Figure 5.7 shows the modified flyback topology which can be used for this purpose.

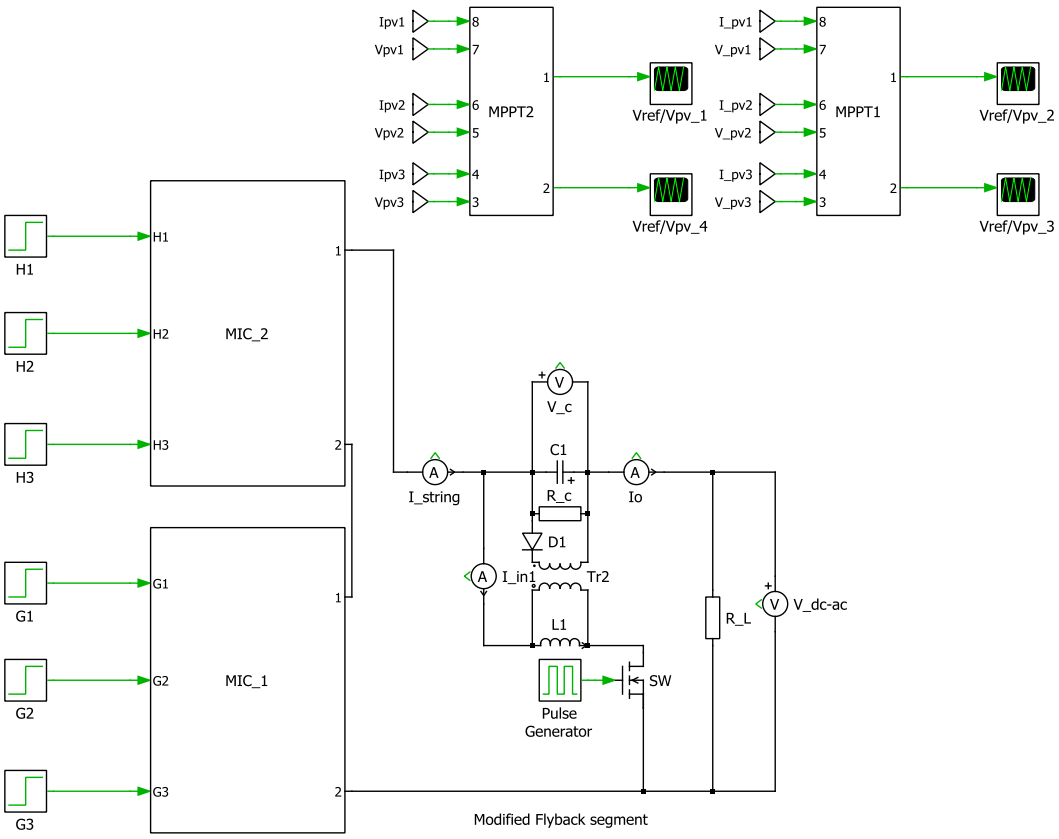

Figure 5.7 Modified flyback dc-dc converter

5.3 Parallel Connected MICs

The parallel connected MICs are fundamentally the same as the series connected MICs with the exception that in this case each MIC is connected to the dc link individually. The opportunity to implement panel level MPPT still exists in the parallel connection. In this configuration and in the following simulation, each MIC is rated to handle the nominal output power of a single panel rated at 250 W. This configuration is more flexible than the series connection as the panel MICs are discretely connected to dc link. Hence in case of a panel or MIC failure, the

power output of other modules can still be transferred to the the dc-ac interconnection. Figure 5.8 shows a parallel MIC system.

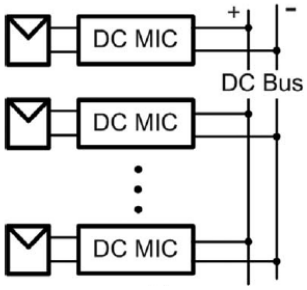

Figure 5.8 Parallel MIC configuration [8]

Parallel MICs have the advantage of performing better during partial shading conditions. During partial shading of a sub-module in a panel, each MIC acts independently with the rest of the system remaining unaffected. Since this is a discreet system, it is not necessary that the PV panels be homogenous [7]. Hence panels of different manufacturers and ratings can be connected to the system. These advantages make the parallel combination of MICs more reliable and tolerant to panel level fault conditions.

Figure 5.9, a part of the simulation, shows a parallel combination of MICs which is connected to the dc inter link regulated at 180 V. This system is compatible for residential rooftops with 120 V ac systems. The dc interconnection in the figure simulates a dc-ac micro-inverter.

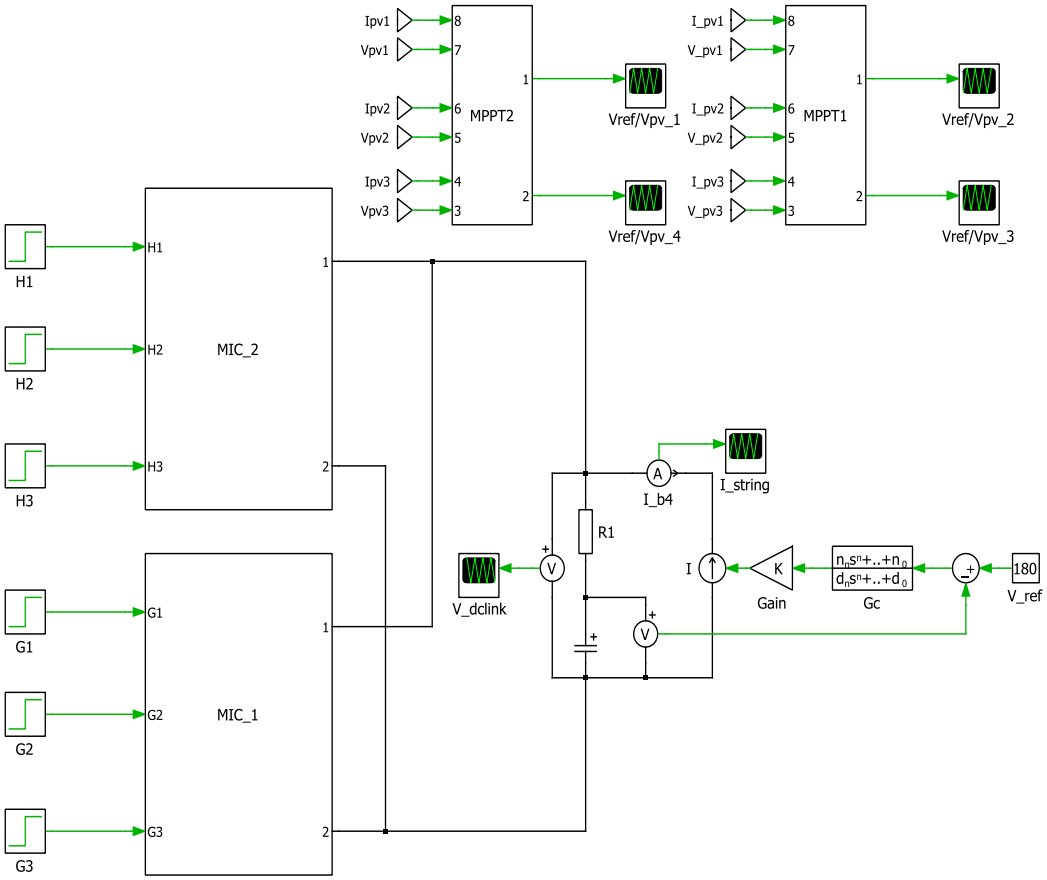

Figure 5.9 parallel MIC configuration used in PLECS

However this configuration has its own drawbacks. Since the MIC connections are in parallel, the voltage of the dc link remains constrained. Unlike the series connection, the dc link voltage cannot be built up to higher values. In order to have high conversion ratio for such system, each MIC will need to have isolated converter topology [8]. This restricts the size of the MIC and puts constraints on its implementation as a panel level or sub-module level solution.

Parallel connected MIC analysis

The figure 5.8 represents the PV sub-module MIC used in the simulation. The analysis extends in the same way as the series combination explained earlier. The irradiance block in MIC_1, G_3 is changed from G =1 to G = 0.5. The Figure 5.10 shows the change in V_{PV} for the partially shaded sub-module with respect to the change in V_{REF} for the particular change in irradiance.

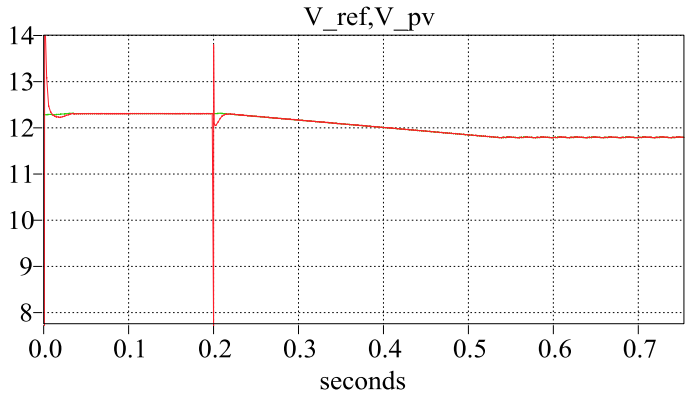

Figure 5.10 V_{PV} and V_{REF} for G=1 to G= 0.5 in parallel MIC

Figure 5.11a and Figure 5.11b show the change in the PV MIC output voltage for each sub-module for the change in irradiance in one sub-module in the parallel panel.

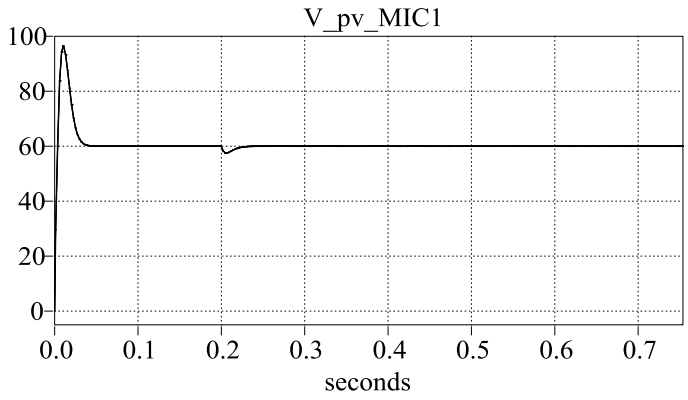

Figure 5.11(a) PV sub-module parallel MIC voltages for the un-shaded panel

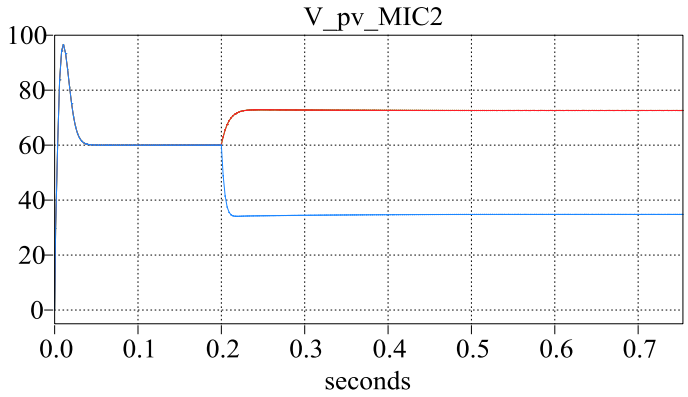

Figure 5.11(b) PV sub-module parallel MIC voltage for partially shaded panel

The total output voltage of the MIC_1 is 180 V after the change in irradiance. The individual voltages of the un-shaded modules in MIC_2 stay regulated at 60 V with the change in irradiance in MIC_1. The total output voltage of the un-shaded MIC_2 is 180 V. Figure 5.12 shows the net change in the dc link voltage after the change in irradiance in MIC_1.

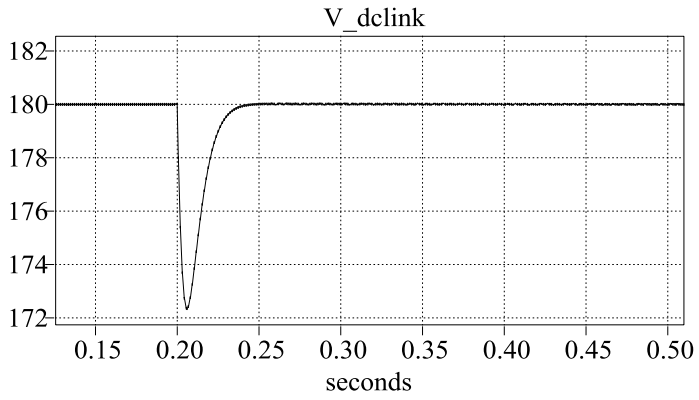

Figure 5.12 DC link voltage with change in irradiance in MIC_1

The duty ratio of the un-shaded and shaded modules needs to be analyzed again. Figure 5.13a and Figure 5.13b show the change in duty ratio in the boost converter in the same MIC for 50% change in irradiance.

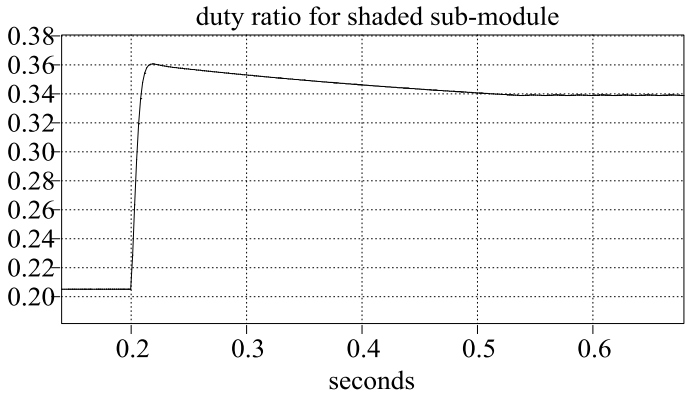

Figure 5.13(a) Change in duty ratio of the boost converter in the MIC_1

The duty ratio of the partially shaded sub-module changes from D= 0.2 to D = 0.34 with the change in irradiance.

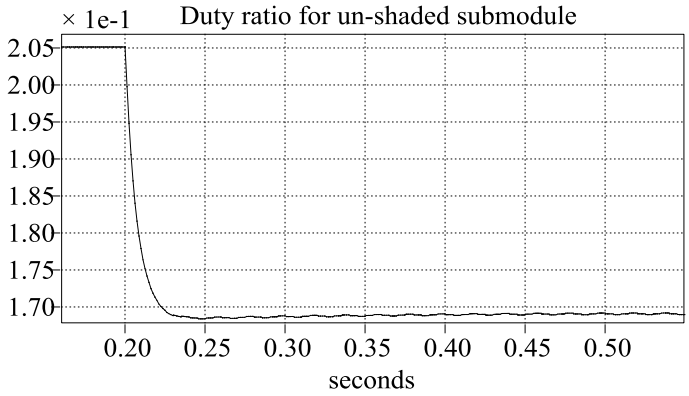

Figure 5.13(b) Change in duty ratio in un-shaded sub-module in MIC_1.

Figure 5.14 shows the change in duty ratio of the un-shaded PV panel. Unlike the series connection, the change in duty ratio is minimal since the MIC_2 output voltage remains regulated with the change in irradiance in the other panel.

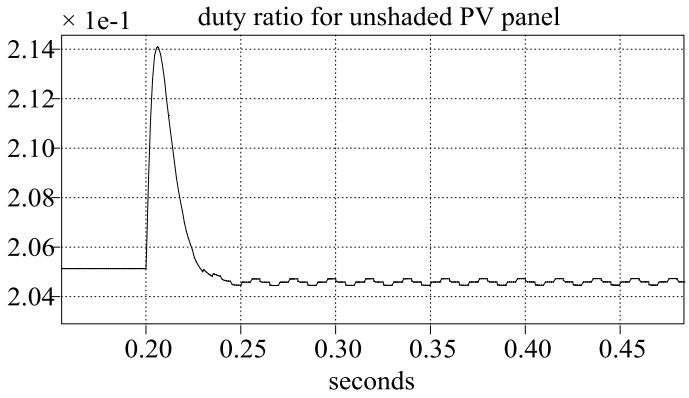

Figure 5.14 Change in duty ratio in un-shaded parallel PV panel

Another factor which needs to be considered is the net dc link current. Unlike the series configuration, the dc link current is the summation of the individual current contributions of the MICs. In this parallel combination, the total dc-link current changes from 2.83A to 2. 58A for 50% drop in irradiance. Figure 5.15 shows the change in current of the system with the irradiance. The net power out of the entire system changes from 510 W to 465 W with the drop in irradiance.

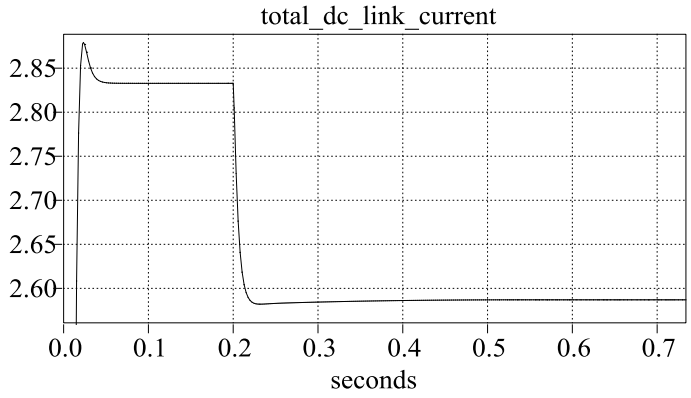

Figure 5.15 Change in net dc link current with irradiance

Chapter 6. Conclusion and future work

In this thesis the main attempt has been to analyse and understand the various dc-dc converters which can be incorporated with the PV modules for residential photovoltaic applications. In this research the major conventional converter topologies which are used in regular practice with the PV module have been studied in great detail. A few novel topologies like switched capacitors and extended duty ratio have also been explored and experimented with.

The boost converter topology has been chosen for detailed analysis and hardware implementation in the PV sub-module level in this thesis. The concept of distributed maximum power point tracking incremental conductance algorithm has also been analysed and simulated at the PV sub-module level. The application of module integrated converters at the PV module level have been around for some time but the aim of this thesis was to analyse the impact on voltage regulation at the dc-ac interconnection of the series or parallel connected MICs without integrating a central dc-dc converter in variable irradiance conditions.

With the addition of the dc link compensator substituting for a micro-inverter at the output node of sub-module MICs series string, it is evident from the simulation results that voltage regulation can be achieved at the dc link interconnection without the addition of any central dc-dc converter. The parallel combination of MICs has also been verified in the simulations. The dc-ac interconnection remains regulated for both the combinations during variable irradiance level.

This finding and simulation results need to substantiated with hardware results. This will form the outline of the future work. The basic groundwork has been laid for the hardware implementation. The e-GAN (enhancement mode Gallium Nitride) switches in the EPC (Efficient Power Conversion) 2001 development board will be used in the hardware implementation of the boost converter. The future could include developing the switched capacitor inductor-less topologies with e-GAN switches for this same PV sub-module application

REFERENCES

[1] U.S. Department of Energy, "SunShot Vision Study," http://www1.eere.energy.gov/solar/pdfs/47927.pdf, February 2012.

[2] N. Femia, G. Petrone, G. Spagnuolo, M. Vitelli, "A Technique for Improving P&O MPPT Performances of Double-Stage Grid-Connected Photovoltaic Systems," IEEE Transactions on Industrial Electronics, vol. 56, issue 11, pp. 4473-4482, Nov. 2009.

[3] N. Femia, G. Petrone, G. Spagnuolo, M. Vitelli, " Optimization of perturb and observe maximum power point tracking method," IEEE Transactions on Power Electronics, vol. 22, issue 4, pp. 963-973, July 2005.

[4] N. Femia, G. Lisi, G. Petrone, G. Spagnuolo, M. Vitelli, "Distributed maximum power point tracking of photovoltaic arrays: novel approach and system analysis," IEEE Transactions on Industrial Electronics, vol. 55, issue 7, pp. 2610-2621, July 2008.

[5] K.H.Hussein, I. Muta, T. Hoshino, M. Osakada, "Maximum photovoltaic tracking: an algorithm for rapidly changing atmospheric conditions," IEE Proceedings – Generation, Transmission and Distribution, vol. 142, issue 142, pp. 59-64, Jan. 1995.

[6] T. Esram, P.L. Chapman, "Comparison of photovoltaic array maximum power point tracking techniques," IEEE Transactions on Energy Conversion, vol. 22, issue 2, pp. 439-449, June 2007.

[7] B. Oraw, R. Ayyanar, "Load adaptive, high eficicency, switched capacitor internmdeiate bus converter," 29th International Telecommunications Energy Conference, 2007, INTELEC 2007, pp. 628-635, Sep/Oct 2007.

[8] Zhigang Liang, Rong Guo, Jun Li, Alex Q. Huang, "A high efficiency pv module-integrated dc/dc converter for pv energy harvest in freedm systems," IEEE Transactions on Power Electronics, vol. 26, issue 3, pp. 897-909, March 2011.

[9] John J. Cooley, Steven B. Leeb, "Per panel photovoltaic energy extraction with multilevel output dc-dc switched capacitor converters," Twenty-Sixth Annual IEEE Applied Power Electronics Conference and Exposition (APEC) 2011, pp. 419-428, March 2011.

[10] Boris Axelrod, Yefim Berkovich, Adrian Ionovici, "Switched-capacitor/switched-inductor structures for getting transformerless hybrid dc-

dc converters," IEEE Transactions on Circuits and Systems I: Regular Papers, vol. 55, issue 2, pp. 687-696, March 2008.

[11] Boris Axelrod, Yefim Berkovich, Adrian Ionovici, "Transformerless dc-dc converters with a very high dc line-to-load voltage ratio," Proceedings of the 2003 International Symposium on Circuits and Systems, 2003, ISACS'03, vol. 3, pp. 435-438, March 2003.

[12] Perry Tsao, Sameh Sarhan, Ismail Jorio, "Distributed max power point tracking for photovoltaic arrays," 2009 34th IEEE Photovoltaic Specialists Conference (PVSC), pp. 2293-2298, June 2009.

[13] Ahmed Elasser, Mohammad Agamy, Juan Sabate, Robert Steigerwald, Rayette Fisher, Maja Harfan-Todorovic, "A comparative study of central and distributed MPPT architectures for megawatt utility and large scale commercial photovoltaic plants," 36th Annual Conference on IEEE Industrial Electronics Society, IECON 2010, pp. 2753-2758, Nov. 2010.

[14] Woo-Young Choi, Ju-Seung Yoo, Jae-Yaeon Choi, "High efficiency dc-dc converter with high step-up gain for low PV voltage sources," 2011 IEEE 8th International Conference on Power Electronics and ECCE Asia (ICPE and ECCE), pp. 1161-1163, May/June 2011.

[15] Wuhua Li, Xiangning He, "Review of nonisolated high step-up dc-dc converters in photovoltaic grid-connected applications," IEEE Transactions on Industrial Electronics, vol. 58, issue 4, pp. 1239-1250, April 2011.

[16] H. Shu-Hung Chung, "Design and analysis of a switched-capacitor-based step-up dc/dc converter with continuous input current," IEEE Transactions on Circuits and Systems I: Fundamental Theory and Applications, vol. 46, issue 6,pp. 722-730, June 1999.

[17] On-Cheong Mak, Yue-Chung Wong, Adrian Ioinovici, "Step-up dc power supply based on a switched-capacitor circuit," IEEE Transactions on Industrial Electronics, vol. 42, issue 1, pp.90-97, Feb. 1995.

[18] Anonymous, U.S. Department of Energy, Energy Efficiency and Renewable Energy, Available at: http://www.eere.energy.gov/basics/renewable_energy/pv_systems.html, visited on June 2012.